Open access • Journal Article • DOI:10.1039/C0EE00260G

Application of cyclic voltammetry to investigate enhanced catalytic current generation by biofilm-modified anodes of Geobacter sulfurreducens strain DL1 vs. variant strain KN400 — Source link

Sarah Strycharz, Anthony P. Malanoski, Rachel M. Snider, Hana Yi ...+2 more authors

Institutions: United States Naval Research Laboratory, University of Massachusetts Amherst

Published on: 01 Mar 2011 - Energy and Environmental Science (The Royal Society of Chemistry)

Topics: Geobacter sulfurreducens, Cyclic voltammetry, Anode, Voltammetry and Cathode

December 21, 2010

Application of Cyclic Voltammetry to Investigate Enhanced Catalytic Current Generation by Biofilm-Modified Anodes of Geobacter Sulfurreducens Strain DL1 vs. Variant Strain Kn400

Sarah M Strycharz
Anthony P Malanoski
Rachel M Snider
Hana Yi
Derek Lovley, *University of Massachusetts - Amherst*, et al.

Energy & Environmental Science

Cite this: *Energy Environ. Sci.*, 2011, **4**, 896

www.rsc.org/ees

PAPER

Application of cyclic voltammetry to investigate enhanced catalytic current generation by biofilm-modified anodes of *Geobacter sulfurreducens* strain DL1 *vs.* variant strain KN400

Sarah M. Strycharz,[a] Anthony P. Malanoski,[a] Rachel M. Snider,[a] Hana Yi,[b] Derek R. Lovley[b] and Leonard M. Tender*[a]

Received 13th July 2010, Accepted 26th October 2010
DOI: 10.1039/c0ee00260g

A biofilm of *Geobacter sulfurreducens* will grow on an anode surface and catalyze the generation of an electrical current by oxidizing acetate and utilizing the anode as its metabolic terminal electron acceptor. Here we report qualitative analysis of cyclic voltammetry of anodes modified with biofilms of *G. sulfurreducens* strains DL1 and KN400 to predict possible rate-limiting steps in current generation. Strain KN400 generates approximately 2 to 8-fold greater current than strain DL1 depending upon the electrode material, enabling comparative electrochemical analysis to study the mechanism of current generation. This analysis is based on our recently reported electrochemical model for biofilm-catalyzed current generation expanded here to a five step model; Step 1 is mass transport of acetate, carbon dioxide and protons into and out of the biofilm, Step 2 is microbial turnover of acetate to carbon dioxide and protons, Step 3 is the non-concerted, 1-electron reduction of 8 equivalents of electron transfer (ET) mediator, Step 4 is extracellular electron transfer (EET) through the biofilm to the electrode surface, and Step 5 is the reversible oxidation of reduced mediator by the electrode. Five idealized voltammetric current *vs.* potential dependencies (voltammograms) are derived, one for when each step in the model is assumed to limit catalytic current. Comparison to experimental voltammetry of DL1 and KN400 biofilm-modified anodes suggests that for both strains, the microbial oxidation of acetate (Step 2) is fast compared to microbial reduction of ET mediator (Step 3), and either Step 3 or EET through the biofilm (Step 4) limits catalytic current generation. The possible limitation of catalytic current by Step 4 is consistent with proton concentration gradients observed within these biofilms and finite thicknesses achieved by these biofilms. The model presented here has been universally designed for application to biofilms other than *G. sulfurreducens* and could serve as a platform for future quantitative voltammetric analysis of non-corrosive anode and cathode reactions catalyzed by microorganisms.

[a]*Center for Biol/Molecular Science and Engineering, Naval Research Laboratory, 4555 Overlook Ave., SW, Washington, DC, 20375, USA. E-mail: tender@nrl.navy.mil*
[b]*Department of Microbiology, Morrill Science Center IV North, University of Massachusetts, Amherst, MA, 01003, USA*

Introduction

Microbial fuel cells (MFCs) exploit the ability of some bacteria to couple oxidation of organic matter with extracellular electron

Broader context

Microbial fuels cells (MFCs) rely on the ability of certain microorganisms to transfer electrons to anodes to catalyze electricity generation from oxidation of biomass. MFCs have thus far been demonstrated to be useful for powering small electronic devices such as a meteorological buoy. Here we present a 5-step model for the microbially catalyzed half-reaction of a MFC based on the voltammetric current-potential dependencies of *G. sulfurreducens* biofilm-modified anodes. The five steps include mass transport of reactants and products into and out of the biofilm, microbial turnover of the fuel source, transfer of electrons from inside the cell to extracellular electron transfer mediators bound into the biofilm, transfer of electrons between the bound mediators, and electron transfer onto the surface of the anode. Our model is broadly applicable and may be useful to develop strategies for optimizing power generation by MFCs.

transfer (EET) to insoluble electron acceptors to catalyze the anode half-reaction.[1–3] In the case of biofilm-modified anodes, membrane-bound proteins, extracellular proteins, and/or soluble redox molecules are thought to mediate EET through the biofilm and across the biofilm/electrode interface to the electrode, which acts as an inexhaustible metabolic electron-acceptor. Extensive research on MFC configuration, source of inoculum, and growth conditions has shown that it is the rate of the microbial-catalyzed anode half-reaction, parameterized as anode current density, which ultimately determines the upper limit of power output.[3–7]

Geobacter species have been shown to dominate anode biofilms enriched under a variety of MFC conditions and from a number of environments, including sediments and wastewater.[8–15] *Geobacter* spp. are unique from other anode-respiring bacteria as they do not appear to rely on soluble redox mediators to transfer electrons to the electrode,[8] and are therefore able to produce current densities higher than any known pure culture microorganism.[4,16,17] As a result, *Geobacter sulfurreducens* has emerged as one of the most widely studied anode-respiring microorganisms.[9,18–25] A complete genome sequence,[26] genome-scale metabolic model,[27] as well as a reliable genetic system,[28] make *G. sulfurreducens* an ideal model microorganism to understand the complex interactions within the anode biofilm resulting in electron transfer to the electrode. Recently, a variant of *G. sulfurreducens*, strain KN400, was selected from a continuously maintained MFC initially inoculated with *G. sulfurreducens* strain DL1, and found to produce approximately 2 to 8-fold the current density of strain DL1 depending upon the electrode material.[16]

Voltammetry is the standard electrochemical technique used to study processes in which an electrode acts as the terminal electron donor or acceptor. In voltammetry, the driving force of the terminal electron-transfer (ET) step is changed by adjusting the electrode potential, while the effect on rate of the overall process is determined by the measured current response. Although cyclic voltammetry (CV) has been used to characterize thermodynamics of the terminal ET step of biofilm catalyzed anode reactions, such as assigning a value for the formal potential of the terminal ET mediator,[22,29] a more complete analysis of the current-electrode potential dependency yielding mechanistic information about the entire catalytic process, which exists for other types of catalyzed electrode reactions, is lacking.[30]

Previously, we proposed a model to describe the voltammetric current-electrode potential dependency exhibited by an idealized *G. sulfurreducens* biofilm-modified anode.[22] Here, we expand upon this model (Fig. 1 and below) to include the effect of mass transport of metabolic reactants and products into and out of the biofilm. We derive 5 idealized voltammetric dependencies, one for when each step in the model is assumed to limit catalytic current while the other steps are assumed to be infinitely fast (*i.e.* limiting case analyses). Qualitative comparison of these simulated voltammograms to experimentally obtained voltammograms of anodes modified with *G. sulfurreducens* strain DL1 and strain KN400 was used to assess the utility of our model to identify possible rate-limiting steps in maximum current generation by electrogenic bacteria, and rationally predict a cause for the finite thickness of anode biofilms. The model presented here derives from earlier models of metabolism of biofilms formed on inert surfaces that rely upon soluble electron acceptors that employ Fick's laws of diffusion to describe mass transport, and

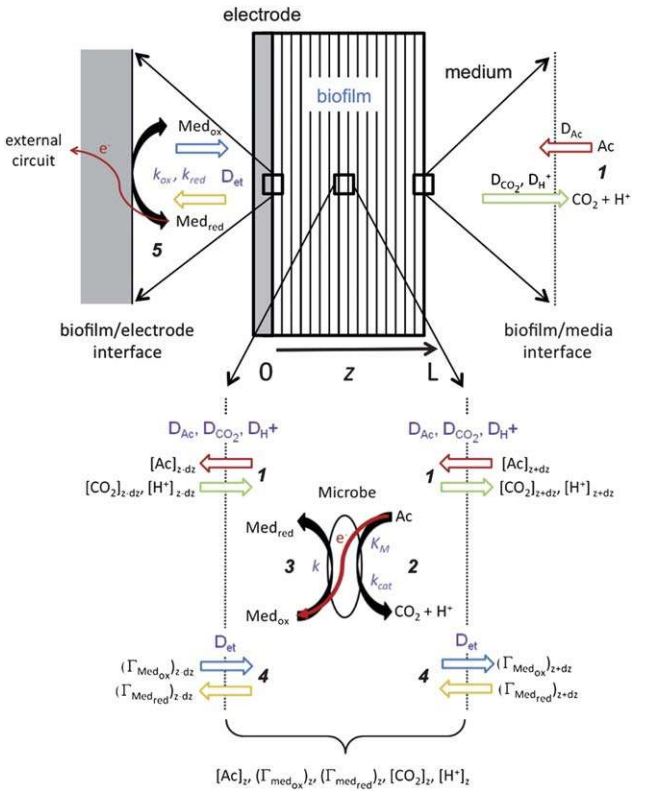

Fig. 1 Schematic representation of model of electrical current generation coupled to acetate oxidation by a biofilm-modified anode. Following the standard strategy for modeling systems involving flux, the biofilm is divided into imaginary thin layers where Fick's 1st law of diffusion is applied to describe the flux of acetate, oxidized and reduced mediator, carbon dioxide, and protons, between adjacent layers and between the outermost layer and media; and Fick's 2nd law of diffusion is applied to describe their change in concentration in each layer over time due their flux. The bold numerals correlate to the reaction steps enumerated in the text. In each layer, the consumption of acetate and oxidized mediator, and generation of reduced mediator, carbon dioxide, and protons, is described by the Michaelis-Menton kinetic model of redox enzymes that utilize electron-transfer mediators. At the electrode surface, it is the reversible oxidation of reduced mediator that results in current. Only acetate, carbon dioxide, and protons are assumed to cross the biofilm/media interface.

Monad/Michaelis-Menton kinetics to describe microbial metabolism.[31–34] More recent models of biofilm current generation by biofilm-modified anodes account for proton mass transport and electrode potential[17,35,36,37] but do not yield voltammetric current-potential dependencies. The model presented here also derives from models of redox enzyme modified-electrodes utilizing co-immobilized ET mediators, owing to similarity of the voltammetric current-electrode potential dependencies of these systems to those of biofilm-modified anodes,[25,29,30,38–40] and to models of electron-transfer through electrode-bound abiotic films containing immobilized electron-transfer mediators.[41]

It is important to note that, as in the above cases, the model presented here assumes that the dominant mode of mass transport and electron-transport is diffusion and not migration. Migration is assumed negligible owing to the underlying assumption of high ionic content of media permeable biofilms[35] and to the ability to

change the net oxidation state of the biofilm from oxidized to reduced during voltammetry. Only recently has migration been incorporated into a model of current generation by biofilm-modified anodes to address mass transport of buffer, but not substrate or products including protons.[35] An investigation of the diffusional nature of electron-transfer within biofilm-modified anodes is currently underway in our laboratory (R. Snider, S. Strycharz-Glaven, L. Tender, manuscript in preparation).

Results and discussion

Electrochemical model of current generation by a biofilm-modified anode

Here we consider an anode-respiring biofilm of *G. sulfurreducens* as a homogeneous, 3-dimensional dispersion of bound (*i.e.* non-diffusing) acetate oxidation enzymes of total thickness L that is divided into imaginary layers of thickness dz where the distance of a given layer from the electrode surface, z, is bound between $z = 0$ (the layer closest the electrode surface/biofilm interface) and $z = L$ (the layer closest the biofilm/medium interface) (Fig. 1).[31,42] It is the oxidation of substrate by microbes in each layer ($0 \leq z \leq L$) coupled to electron transfer to the electrode surface integrated across the biofilm which results in catalytic current generation by the entire biofilm. The steps describing the contribution to current by microbes in a given layer are as follows (Fig. 1).

Step 1. $\mathrm{Ac}^{*} \xrightarrow{D_{AC}} \mathrm{Ac}_z, (2\mathrm{CO}_2 + 8\mathrm{H} +)_z \xrightarrow{D_{CO_2}, D_{H^+}} \left(2\mathrm{CO}_2 + 8\mathrm{H}^{+}\right)^{*}$

Step 2. $\mathrm{Mic}_{ox} + \mathrm{Ac} \overset{K_M}{\rightleftharpoons} \mathrm{Mic}_{ox-Ac} + \mathrm{H_2O} \xrightarrow{k_{cat}} \mathrm{Mic}_{red} + 2\mathrm{CO}_2 + 8\mathrm{H}^{+}$

Step 3. $\mathrm{Mic}_{red} + 8(\mathrm{Med}_{ox})_z \overset{k}{\rightleftharpoons} \mathrm{Mic}_{ox} + 8(\mathrm{Mic}_{red})_z$

Step 4. $8(\mathrm{Med}_{red})_z + 8(\mathrm{Med}_{ox})_{z-dz} \overset{D_{et}}{\rightleftharpoons} 8(\mathrm{Med}_{ox})_z + 8(\mathrm{Med}_{red})_{z-dz}$

Step 5. $8(\mathrm{Med}_{red})_0 \overset{k_{ox}(E), k_{red}(E)}{\rightleftharpoons} 8(\mathrm{Med}_{ox})_0 + 8e -$ (at the anode)

Step 1 is mass transport of acetate, carbon dioxide and protons between the medium at distance z parameterized by diffusion coefficients D_{Ac},D_{CO_2},and D_{H^+}.[37] Step 2 is microbial turnover of acetate to carbon dioxide and protons. Step 2 is assumed to follow the Michaelis–Menten kinetic model and is parameterized by microbial affinity for acetate (K_M) and a rate constant for the turnover of acetate to products yielding 8 electrons per equivalent of Ac oxidized (k_{cat}).[43] With respect to the simple reaction scheme presented here, the Michaelis–Menten kinetic model yields identical dependencies to the Monod kinetic model often invoked to describe biofilm substrate consumption.[35,42] Step 3 is the non-concerted, 1-electron reduction of 8 equivalents of ET mediator (assuming 100% coulombic efficiency) parameterized by the rate constant k. Previous fitting of cyclic voltammetry of a DL1-biofilm modified anode suggests that one electron at a time is transferred from a reduced microbe to an oxidized mediator (*i.e.* $n = 1$).[22] The use of a first order reaction for Step 3 follows directly from models of redox enzyme electrodes[25,29,30,38–40] and is consistent with the supposition that mediators in Step 3 are bound to the microbe surface (*e.g.* outer membrane cytochromes).[22] Step 4 is EET through the biofilm from distance z to the electrode surface by either a diffusing mediator or a series of sequential ET reactions (*i.e.* electron hopping) among adjacent bound mediators as exhibited by redox-polymer-modified electrodes,[41,44–46] both parameterized by an effective electron diffusion coefficient (D_{et}). Step 4 applies equally for bound and diffusing mediators, even though *G. sulfurreducens* is assumed to utilize bound mediators.[22,29] Regardless of whether a mediator is bound or diffusing, reducing equivalents (electrons) propagating to the electrode reside on reduced mediator while oxidizing equivalents (electron holes) propagating away from the electrode reside on oxidized mediator and both ET mechanisms are described as diffusional processes.[41,47] Step 5 is the reversible oxidation of reduced mediator by the electrode, parameterized by the mediator formal potential ($E^{o'}$) and heterogeneous electron-transfer rate constants for the forward and reverse reactions ($k_{ox}$and k_{red}) that are dependent on the electrode potential. Steps 3, 4 and 5 collectively constitute the EET process to the anode.

As described above and depicted in Fig. 1, electricity generation results from oxidation of reduced mediator at the electrode surface when the electrode potential is at a sufficiently oxidizing potential (Step 5). This catalytic current is sustained by the flux of electrons (reduced mediators) toward the electrode surface (Step 4) generated by the microbes in the biofilm (Step 3). Step 3 is in turn sustained by the flux of electron holes (oxidized mediators) into the biofilm (Step 4) generated at the electrode surface (Step 5), and by the turnover of acetate (Step 2), which in turn, is sustained by the flux of acetate into the biofilm (Step 1). It is important to note that this model is not specific to biofilm-modified anodes. It is equally applicable to biofilm-modified cathodes by reversing Steps 1–5 and replacing the electron donating substrate (acetate) with an electron accepting substrate (*e.g.* fumarate)[48] (Strycharz *et al.*, manuscript in preparation).

Derivation of simulated voltammetry of a biofilm-modified anode

When performing a voltammogram, i (current) is recorded while E (the electrode potential) is changed linearly with time at rate v (scan rate) from E_{init} (initial potential) as described by eqn (1).

$$E = E_{init} + vt \tag{1}$$

where

$$v = \frac{dE}{dt} \tag{2}$$

With respect to the experimental cyclic voltammetry depicted below, a cathodic scan (*i.e.* $v < 0$) was first recorded, from $E_{init} =$ 0.300 V *vs.* Ag/AgCl until $E = -0.800$ V *vs.* Ag/AgCl, immediately

followed by an anodic scan (*i.e.*, $v>0$), from $E_{init}= -0.800$ V *vs.* Ag/AgCl until $E = 0.300$ V *vs.* Ag/AgCl. With respect to the simulated cyclic voltammetry depicted below, a cathodic scan was first determined, from $E_{init} = 0.300$ V *vs.* $E^{o'}$ until $E = -0.300$ V *vs.* $E^{o'}$, immediately followed by an anodic scan, from $E_{init}= -0.300$ V *vs.* $E^{o'}$ until $E = 0.300$ V *vs.* $E^{o'}$. Based on the above model,

$$i = nFA[k_{ox}(\Gamma_{\mathrm{Med_{red}}})_0 - k_{red}(\Gamma_{\mathrm{Med_{ox}}})_0] \quad (3)$$

where current is proportional to the instantaneous rate of Step 5; assumed here to be a reversible 1st order reaction in which one of the products is an electron on the electrode surface,[47] and where $(\Gamma_{\mathrm{Med_{red}}})_0$ and $(\Gamma_{\mathrm{Med_{ox}}})_0$ are the instantaneous concentrations of reduced and oxidized ET mediator in the biofilm layer closest to the electrode surface ($z = 0$). The forward and reverse rate constants, k_{ox} and k_{red}, are dependent upon E as traditionally described by the Butler-Volmer rate expressions:[47,49]

$$k_{ox} = k^0 e^{[(1-\alpha)f(E-Eo')]} \quad (4)$$

$$k_{red} = k^0 e^{[-\alpha f(E-Eo')]} \quad (5)$$

where k^0 is the standard rate constant (when $E = E^{o'}$) and α is the transfer coefficient ($0 \le \alpha \le 1$, typically 0.5). Eqn (4) and (5) indicate that as E is made more positive, k_{ox} increases exponentially while k_{red} decreases exponentially and *vice versa* as E is made more negative. $(\Gamma_{\mathrm{Med_{red}}})_0$ and $(\Gamma_{\mathrm{Med_{ox}}})_0$ are dependent on the flux of $\mathrm{Med_{red}}$ into layer $z = 0$ from layer $z = dz$ (next closest layer to the electrode surface), and the flux of $\mathrm{Med_{ox}}$ out of layer $z = 0$ into layer $z = dz$. Considering $\mathrm{Med_{red}}$ first, following Fick's 1st law of diffusion,[47] its flux between these layers is dependent on the difference in its concentration in these layers. Following Fick's 2nd law of diffusion,[47] its concentration in these layers changes at a rate that is dependent on its flux into and out of these layers. Since the flux of $\mathrm{Med_{red}}$ into and out of layer $z = dz$ is dependent on its flux into and out of layer $z = 2dz$, which in turn is dependent on its flux into and out of layer $z = 3dz$, *etc.*, its flux into layer at $z = 0$ is dependent on its flux into and out of each layer of the biofilm ($0 \le z \le L$), and its concentration in layer $z = 0$ is dependent on its concentration in each layer of the biofilm. The pertinent equations used to describe the instantaneous concentration of $\mathrm{Med_{red}}$ in each layer of the biofilm and therefore in layer $z = 0$ are:

$$for\ 0 \le z < L, \quad \frac{d(\Gamma_{\mathrm{Med_{red}}})_z}{dt} = (J_{\mathrm{Med_{red}}})_z + (S_{\mathrm{Med_{red}}})_z \quad (6)$$

Where

$$(J_{\mathrm{Med_{red}}})_z = \left[D_{et}\frac{d(\Gamma_{\mathrm{Med_{red}}})_{z-dz}}{dz} - D_{et}\frac{d(\Gamma_{\mathrm{Med_{red}}})_{z+dz}}{dz}\right] = D_{et}\frac{d^2(\Gamma_{\mathrm{Med_{red}}})_z}{dz^2} \quad (7)$$

and

$$(S_{\mathrm{Med_{red}}})_z = \frac{k_{cat}(\Gamma_{\mathrm{Mic}})_z}{\left[1 + \frac{k_{cat}}{k(\Gamma_{\mathrm{Med_{ox}}})_z} + \frac{K_M}{8[Ac]_z}\right]} \quad (8)$$

where $(J_{\mathrm{Med_{red}}})_z$ is the difference in flux of $\mathrm{Med_{red}}$ into layer z from layer $z + dz$ and from layer z to layer $z - dz$. $(S_{\mathrm{Med_{red}}})_z$ is the collective metabolic activity of microbes in layer z described by their collective rate of generation of $\mathrm{Med_{red}}$. $(S_{\mathrm{Med_{red}}})_z$ is derived directly from the Michaelis–Menten kinetic model of a redox enzyme-modified electrode that utilizes ET mediators, where the factor 8 results from the 8 : 1 ratio of $\mathrm{Med_{red}}$ generated per equivalent of acetate oxidized [30,43]; and $(\Gamma_{\mathrm{Mic}})_z$, $(\Gamma_{\mathrm{Med_{ox}}})_z$ and $[Ac]_z$ are the concentrations of microbes, oxidized mediator, and acetate in layer z. Eqn (9) describes the boundary condition in which $\mathrm{Med_{red}}$ is confined to the biofilm. Eqn (10) describes conservation of mass in which the total concentration of mediator in each layer is the sum of mediator in the oxidized and reduced forms in each layer (assumes mediator is bound within the biofilm and does not diffuse). Eqn (11) describes the resulting concentration of $\mathrm{Med_{ox}}$ across the biofilm, in which the balance of mediator not in the reduced form in a given layer is in the oxidized form. $\mathrm{Med_{ox}}$ generated at the electrode surface induces a flux of $\mathrm{Med_{ox}}$ into the biofilm resulting in a concentration gradient of $\mathrm{Med_{ox}}$ across the biofilm. Owing to conservation of mass, the $\mathrm{Med_{ox}}$ concentration gradient is the inverse of the concentration gradient of $\mathrm{Med_{red}}$ across the biofilm.

$$for\ z < 0\ and\ z > L,\ (\Gamma_{\mathrm{Med_{red}}})_z = 0 \quad (9)$$

$$(\Gamma_{\mathrm{Med}})_z = (\Gamma_{\mathrm{Med_{ox}}})_z + (\Gamma_{\mathrm{Med_{red}}})_z \quad (10)$$

$$for\ 0 \le z < L, \quad \frac{d(\Gamma_{\mathrm{Med_{ox}}})_z}{dz} = \frac{-d(\Gamma_{\mathrm{Med_{red}}})_z}{dz} \quad (11)$$

The dependence of eqn (8) on $[Ac]_z$ makes it necessary to determine the flux of acetate across each layer of the biofilm in order to determine $(S_{\mathrm{Med_{red}}})_z$ throughout the biofilm. The pertinent equations below are analogous to those above, with the exception that the acetate concentration in medium adjacent to the biofilm is assigned the bulk medium acetate concentration, $[Ac]^*$:

$$for\ 0 < z < L, \frac{d[Ac]_z}{dt} = (J_{\mathrm{Ac}})_z + (S_{\mathrm{Ac}})_z \quad (12)$$

$$(J_{\mathrm{Ac}})_z = \left[D_{et}\frac{d[Ac]_{z-dz}}{dz} - D_{et}\frac{d[Ac]_{z+dz}}{dz}\right] = D_{Ac}\frac{d^2[Ac]_z}{dz^2} \quad (13)$$

$$(S_{\mathrm{Ac}})_z = \frac{-k_{cat}(\Gamma_{\mathrm{Mic}})_z}{8\left[1 + \frac{k_{cat}}{k(\Gamma_{\mathrm{Med_{ox}}})_z} + \frac{K_M}{8[Ac]_z}\right]} \quad (14)$$

$$for\ z < 0,\ [Ac]_z = 0;\ for\ z > L,\ [Ac]_z = [Ac]^* \quad (15)$$

where $(S_{\mathrm{Ac}})_z$ is the collective metabolic activity of microbes in a layer at distance z described by their collective rate of acetate consumption. Step 2 results in the irreversible generation of 8 protons per equivalent of acetate oxidized. Assuming that the generation of protons does not inhibit the rate of Step 2, that the mass transport of protons out of the biofilm in the medium is affected by diffusion, and that concomitantly generated carbon dioxide does not act as a buffer, the pertinent equations below describe the concentration of protons in each layer of the biofilm

$$for\ 0 < z < L, \frac{d[H^+]_z}{dt} = (J_{H^+})_z + (S_{H^+})_z \quad (16)$$

$$(J_{H^+})_z = \left[D_{H^+}\frac{d[H^+]_{z-dz}}{dz} - D_{H^+}\frac{d[H^+]_{z+dz}}{dz}\right] = D_{H^+}\frac{d^2[H^+]_z}{dz^2} \quad (17)$$

$$(S_{H^+})_z = \frac{k_{cat}(\Gamma_{\mathrm{Mic}})_z}{\left[1 + \frac{k_{cat}}{k(\Gamma_{\mathrm{Med_{ox}}})_z} + \frac{K_M}{8[Ac]_z}\right]} \quad (18)$$

$$for\ z < 0,\ [H^+]_z = 0;\ for\ z > L,\ [H^+]_z = [H^+]^* \quad (19)$$

where $(S_{H^+})_z$ is the collective metabolic activity of microbes in a layer at distance z described by their collective rate of generation of protons. If, in addition, the medium contains a buffer,[6,35] then the additional pertinent equations are:

$$for\ 0 < z < L\ and\ B + H^+ \rightleftarrows BH^+,\ K_{eq} = \frac{[BH^+]_z}{[B]_z[H^+]_z} \quad (20)$$

$$(J_B)_z = \left[D_B\frac{d[B]_{z-dz}}{dz} - D_B\frac{d[B]_{z+dz}}{dz}\right] = D_B\frac{d^2[B]_z}{dz^2} \quad (21)$$

$$(J_{BH^+})_z = \left[D_{BH^+}\frac{d[BH^+]_{z-dz}}{dz} - D_{BH^+}\frac{d[BH^+]_{z+dz}}{dz}\right] = D_{BH^+}\frac{d^2[BH^+]_z}{dz^2} \quad (22)$$

$$for\ z < 0,\ [B]_z = 0\ and\ [BH^+]_z = 0;\ for\ z > L,\ [B]_z = [B]^*\ and\ [H^+]_z = [H^+]^* \quad (23)$$

where $[B]_z$ and $[BH^+]_z$ are the concentrations of unprotonated and protonated buffer in each layer of the biofilm, and K_{eq} is the protonation equilibrium constant. Here, unprotonated buffer diffuses into the biofilm from the medium, is protonated, and diffuses out; reducing the proton concentration within the biofilm and affecting mass transport of a portion of the protons out of the biofilm.

Simulated idealized voltammetry under non-turnover conditions

An explicit solution to eqn (3) requires simultaneous solution of the above flux equations, which is only possible for very limited cases. It is instructive to consider a special condition in which Step 5 is at equilibrium, defined by eqn (24).

$$k_{ox}(\Gamma_{\mathrm{Med_{red}}})_0 = k_{red}(\Gamma_{\mathrm{Med_{ox}}})_0 \quad (24)$$

Substitution for k_{ox} and k_{red} by eqn (4) and 5 and rearrangement yields the Nernst equation (eqn (25)), which provides the equilibrium values of reduced and oxidized mediator layer $z = 0$ as a function of the electrode potential and the total mediator at concentration regardless of oxidation state in layer $z = 0$ (eqn (26) and (27)).

$$\frac{(\Gamma_{\mathrm{Med_{red}}})_0}{(\Gamma_{\mathrm{Med_{ox}}})_0} = e^{\left[\frac{(E-E^{o'})}{f}\right]} \quad (25)$$

$$(\Gamma_{\mathrm{Med_{red}}})_0 = \frac{(\Gamma_{\mathrm{Med}})_0}{1+X} \quad (26)$$

$$(\Gamma_{\mathrm{Med_{ox}}})_0 = \frac{(\Gamma_{\mathrm{Med}})_0 X}{1+X} \quad (27)$$

where

$$X = e^{\left[\frac{(E-E^{o'})}{f}\right]} \quad (28)$$

When Step 5 is at equilibrium, eqn (26) and (27) indicate that $(\Gamma_{\mathrm{Med_{red}}})_0 = 0$ and $(\Gamma_{\mathrm{Med_{ox}}})_0 = (\Gamma_{\mathrm{Med}})_0$ when $E \gg E^{o'}$, $(\Gamma_{\mathrm{Med_{red}}})_0 = (\Gamma_{\mathrm{Med}})_0/2$ and $(\Gamma_{\mathrm{Med_{ox}}})_0 = (\Gamma_{\mathrm{Med}})_0/2$ when $E = E^{o'}$, and $(\Gamma_{\mathrm{Med_{red}}})_0 = (\Gamma_{\mathrm{Med}})_0$, and $(\Gamma_{\mathrm{Med_{ox}}})_0 = 0$, when $E \ll E^{o'}$.

If not at equilibrium, Step 5 will tend toward equilibrium at a rate that is dependent on k_{ox} and k_{red} (which scale with k^0 for a given value of E) and on v since the equilibrium condition constantly changes as E changes. This process results in a contribution to current (i_{dE}) obtained by solution of eqn (3) as $(\Gamma_{\mathrm{Med_{red}}})_0$ and $(\Gamma_{\mathrm{Med_{ox}}})_0$ tend toward their E-dependent equilibrium values where electrons required to convert Med_{red} to Med_{ox} or *vice versa* are accepted or donated by the electrode. When $v = 0$, $i_{dE} = 0$, since Step 5 is assumed to be at steady state and the balance of current, i_{cat}, where $i = i_{cat} + i_{dE}$, is due to biofilm catalyzed oxidation of acetate. If k^0 is sufficiently large such that Step 5 is sufficiently fast with respect to v, Step 5 will be nearly at equilibrium for each value of E while recording a voltammogram with $(\Gamma_{\mathrm{Med_{red}}})_0$ and $(\Gamma_{\mathrm{Med_{ox}}})_0$ assumed to directly depend on each value of E as described by eqn (26) and (27). If Step 4 is also sufficiently fast with respect to v, then the concentrations of reduced and oxidized mediator across the entire biofilm ($0 \le z \le L$) are uniform and assumed to directly depend on E

$$\Gamma_{\mathrm{Med_{red}}} = \frac{\Gamma_{\mathrm{Med}}}{1+X} \quad (29)$$

$$\Gamma_{\mathrm{Med_{ox}}} = \frac{\Gamma_{\mathrm{Med}} X}{1+X} \quad (30)$$

where $\Gamma_{\mathrm{Med_{red}}}$, $\Gamma_{\mathrm{Med_{ox}}}$, and Γ_{Med} are the total concentrations of reduced, oxidized and total mediator for the entire biofilm and X is defined in eqn (28). Under these conditions, each incremental change in E while recording a voltammogram (dE) results in an incremental change in $\Gamma_{Med_{red}}$ and $\Gamma_{Med_{red}}$ and the resulting contribution to current (i_{dE}) can be expressed explicitly as:

$$i_{dE} = nFA\left(\frac{d\Gamma_{Med_{ox}}}{dt}\right)_{dE} = nFA\left(\frac{d\Gamma_{Med_{ox}}}{dX}\right)_{dE}\left(\frac{dX}{dE}\right)\left(\frac{dE}{dt}\right) = \frac{nfFAv\Gamma_{Med}(X)}{(1+X)^2} \quad (31)$$

where

$$\left(\frac{d\Gamma_{Med_{ox}}}{dX}\right)_{dE} = \frac{\Gamma_{Med}}{(1+X)^2} \quad and \quad \frac{dX}{dE} = fX \tag{32}$$

The current, described by eqn (31) (depicted graphically in Fig. 2), is the well-known *i vs. E* (*E*, *v*) voltammetric dependency (voltammetric scan rate dependency) for electrochemical systems described by fast Steps 4 and 5, that are non-catalytic (*i.e.* lacking Steps 1 – 3). Such systems include thin layer electrochemical cells[47] and chemically modified electrodes.[47,49,50] With respect to biofilm-modified anodes, this dependency is representative of an idealized biofilm-modified anode in the absence of the electron donor (*e.g.* acetate). In Fig. 2, when the initial potential is 0.3 V *vs.* $E^{o'}$, all of the mediator is in the oxidized state. For a given scan rate, as *E* is changed from 0.3 V to −0.3 V *vs.* $E^{o'}$, $\frac{dE}{dt} < 0$ and negative (cathodic) current occurs resulting from ET from the electrode converting oxidized to reduced mediator. As *E* approaches $E^{o'}$, each incremental change in *E* requires a greater amount of oxidized mediator be converted to reduced mediator resulting in an increasing cathodic current. As *E* passes $E^{o'}$, each incremental change in *E* requires a smaller amount of oxidized mediator be converted to reduced mediator resulting in a decreasing cathodic current. When the electrode potential is at −0.3 V *vs.* $E^{o'}$, all of the mediator is in the reduced form and no current flows. For the anodic scan, the initial potential is −0.3 V *vs.* $E^{o'}$. As the electrode potential is changed back to 0.3 V *vs.* $E^{o'}$, $\frac{dE}{dt} > 0$ and positive (anodic) current occurs indicating ET to the electrode from mediator in the biofilm converting reduced mediator to oxidized mediator in an analogous fashion as above. Since the total amount of mediator is constant, increasing the scan rate increases the magnitude of current since less time is utilized to pass the same amount of charge. Notable features of voltammetry described by eqn (31) (derived for when Steps 4 and 5 are considered very fast) are peak current densities ($j_{P,A}$,$j_{P,C}$) that scale linearly with *v* and Γ_{Med} and peak potentials ($E_{P,A}$,$E_{P,C}$) = $E^{o'}$ for all values of *v* (Fig. 2 insets).

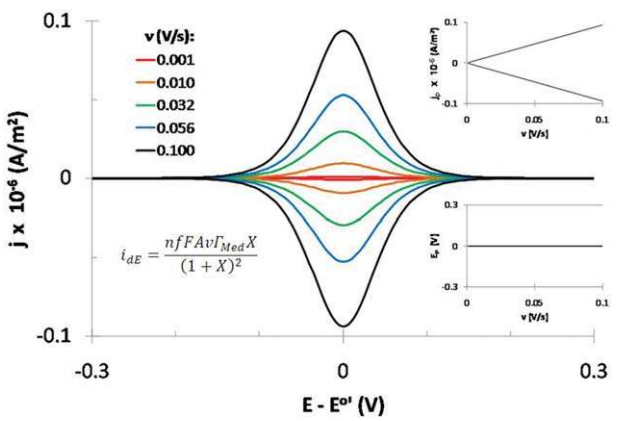

Fig. 2 Representative calculated cyclic voltammetry as a function of scan rate in absence of acetate based on eqn (31) where current (i_{dE}) results from the changing oxidation state of the electron transfer mediator throughout the biofilm due to the changing electrode potential. Insets depict the calculated anodic and cathodic peak current density ($j_{P,A}$,$j_{P,C}$) and peak potential ($E_{P,A}$,$E_{P,C}$) dependency on scan rate. Values of parameters used: $A = 1$ cm^2, $\Gamma_{Med} = 1.$ mole cm^{-2}, $T = 298$ K.

Rate-limiting cases for biofilm-catalyzed anodic current

Here we consider five cases, one for when each reaction step is assumed to limit catalytic current while the remaining steps are assumed to be infinitely fast, and there is excess acetate such that catalytic current (i_{cat}) at $E \gg E^{o'}$ is independent of [*Ac*]*. We derive idealized voltammetric current *vs.* potential dependencies for each case based on the above equations. It is important to note that the values of the parameters used to generate these dependencies do not reflect real values but were chosen to illustrate voltammetric features and trends. We do not attempt to fit the experimental voltammograms with realistic values for the parameters owing to the multi-parameter nature of such fits.

Case 1: catalytic current limited by Step 1. Finite rates of mass transport of the microbial metabolic reactant (acetate) and products (carbon dioxide and protons) are expected to result in transient concentration gradients of these species across a biofilm during voltammetry. Considering acetate as representative, the concentration of acetate inside the biofilm at a given distance from the electrode surface, $[Ac]_z$, will decrease as $z \to 0$ (for microbes closer to the electrode surface) due to its supply from the medium and its consumption by microbes within the biofilm/medium interface. If the acetate concentration gradient is negligible such that $K_M \ll 8[Ac]_z$ is valid throughout the biofilm (eqn (8)), and if the rates of Steps 4 and 5 are very fast such that the concentration of oxidized mediator throughout the biofilm is uniform and described by eqn (30), then eqn (8) simplifies:

$$S_{\mathrm{Med_{red}}} = \int_0^L \left(S_{\mathrm{Med_{red}}}\right)_z = \frac{k_{cat}\Gamma_{\mathrm{Mic}}}{\left[1 + \frac{k_{cat}}{k\Gamma_{\mathrm{Med_{ox}}}}\right]} = \frac{k_{cat}\Gamma_{\mathrm{Mic}}}{\left[1 + \frac{k_{cat}}{k\Gamma_{\mathrm{Med}}\frac{X}{1+X}}\right]} \tag{33}$$

where $S_{\mathrm{Med_{red}}}$ is the rate of generation of reduced mediator by the entire biofilm. Since 4 and 5 are considered to be infinitely fast, solution of eqn (3) yields:

$$i = i_{cat} + i_{dE} = \frac{nfAk_{cat}\Gamma_{\mathrm{Mic}}}{\left[1 + \frac{k_{cat}}{k\Gamma_{\mathrm{Med}}\frac{X}{1+X}}\right]} + \frac{n^2F^2Av\Gamma_{Med}(X)}{RT(1+X)^2} \tag{34}$$

where current is the sum of a contribution that is proportional to the rate of generation of reduced mediator by the entire biofilm (i_{cat}), and a contribution due to the changing concentration of reduced mediator in the biofilm due to the changing electrode potential (i_{dE}). If instead, the acetate concentration gradient is appreciable such that $K_M \gg 8[Ac]$ as $z \to 0$, it is not possible to derive an expression for the full *i vs. E* and *v* voltammetric scan rate dependency as above (eqn (34)). Instead, a *i vs. E* dependency for $v \to 0$ (slow scan voltammetry) can be approximated numerically by determining current for each value of *E* when $v = 0$ (steady state approximation where all concentration gradients in the biofilm are assumed to be constant with time and $i_{dE} = 0$) by setting $\frac{d(\Gamma_{\mathrm{Med_{red}}})_z}{dt} = 0$ and $\frac{d[Ac]_z}{dt} = 0$. Fig. 3A and 3B depict representative calculated acetate concentration gradients based on the numerical solution of eqn (14) when $v = 0$ as a function of D_{Ac} and select values of *E* when $\frac{k_{cat}}{k\Gamma_{Med}} = 1000$ (*i.e.* rate of Step 2

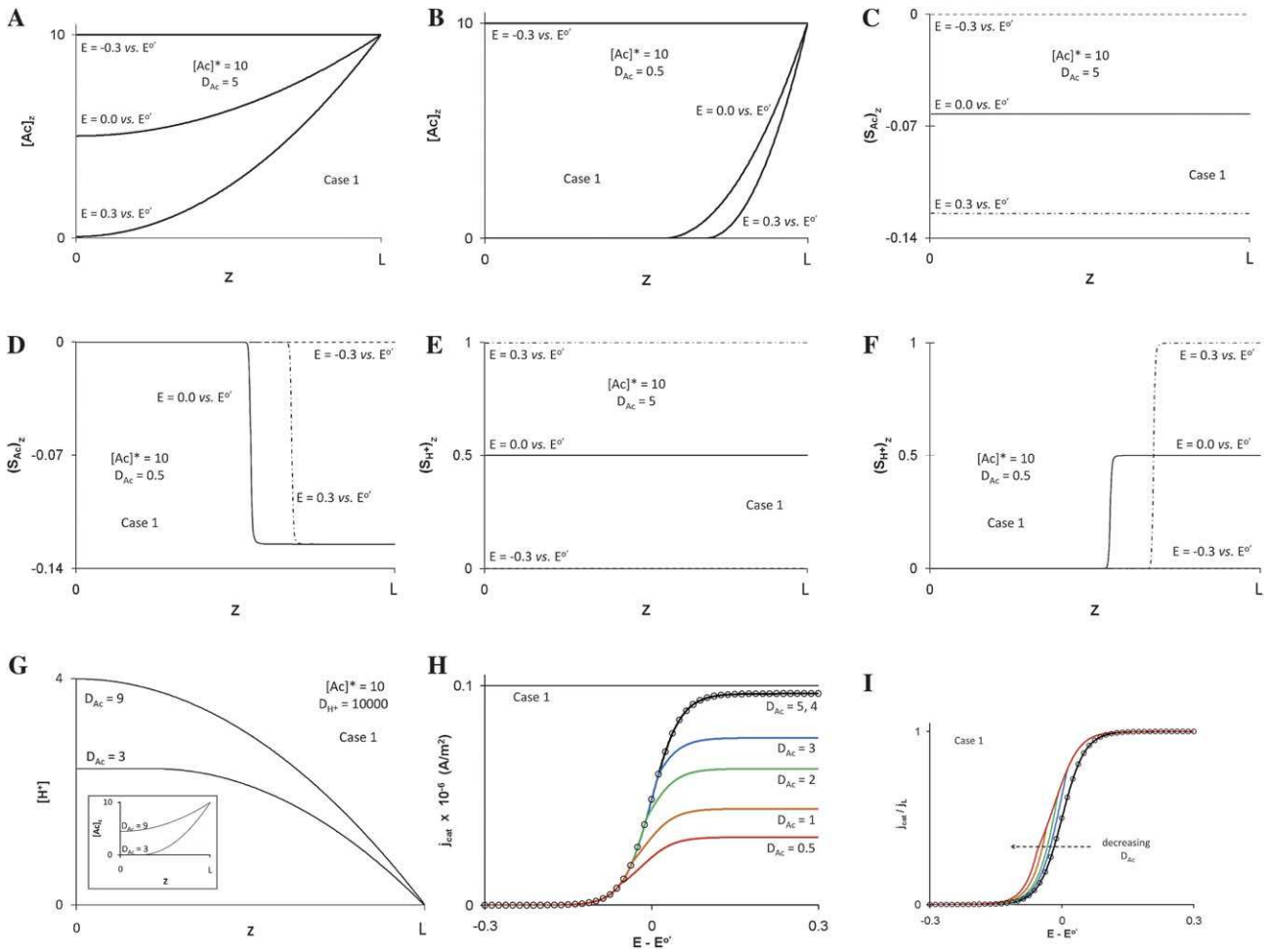

Fig. 3 **(A and B).** Representative calculated steady-state acetate concentration gradients as a function of electrode potential (E) and the acetate diffusion coefficient (D_{Ac}) based on Case 1. Horizontal axis is distance inside biofilm from the electrode surface (units of cm). When values of other parameters are maintained constant, a smaller value of D_{Ac} and a more positive value of E predicts a steeper acetate concentration gradient towards the electrode surface. Values of other parameters used: $A = 1$ cm^2, $\Gamma_{Mic} = 1$ mole cm^{-2}, $\Gamma_{Med} = 1$ mole cm^{-2}, $[Ac]^* = 10$ mole cm^{-3}, $K_M = 1$ mole cm^{-3}, $k_{cat} = 1000$ s^{-1}, $k = 1$ mole^{-1} cm^2 s^{-1}, $k^0 = 10\,000$ s^{-1}, $T = 298$ K. **(C and D).** Corresponding representative calculated steady-state rate of acetate consumption gradients based on Case 1. Horizontal axis is distance inside biofilm from the electrode surface (units of cm). In the case of Fig. 3C, acetate depletion depicted in Fig. 3A with decreasing distance to the electrode surface is not sufficient even at $E = 0.3$ V to affect rate of acetate consumption, since $K_M \ll 8[Ac]_z$ throughout the biofilm. In the case of Fig. 3D, acetate depletion depicted in Fig. 3B is sufficient to affect rate of acetate consumption within the biofilm owing to the lower value of D_{Ac}. Assuming all cells in a biofilm are metabolically active, Case 1 predicts a finite biofilm thickness limited by the diffusion depth of acetate from the medium. **(E and F).** Corresponding representative calculated steady-state rate of proton generation gradients based on Case 1. Horizontal axis is distance inside biofilm from the electrode surface (units of cm). **(G).** Representative calculated steady-state proton concentration gradients based on Case 1 at $E = 0.3$ V when acetate depletion is appreciable due to a relatively small acetate diffusion coefficient ($D_{Ac} = 3$ cm^2 s^{-1}), and when acetate depletion is not appreciable due to a relatively large acetate diffusion coefficient ($D_{Ac} = 9$ cm^2 s^{-1}). The vertical axis is proton concentration in biofilm *vs.* proton concentration in medium. Horizontal axis is distance inside biofilm from the electrode surface (units of cm). **Inset**: corresponding acetate concentration gradients. Values of other parameters used same as Fig. 3A–3F. **(H and I).** Representative calculated steady-state slow scan cyclic voltammograms (for $v \rightarrow 0$) as a function of the acetate diffusion coefficient (D_{Ac}, units of cm^2 s^{-1}) based on Case 1. (○): Fit to voltammogram when $D_{Ac} = 5$ cm^2 s^{-1} based on eqn (37) where the midpoint potential (E_M) is equal to the mediator formal potential ($E^{o'}$), and the limiting current density ($j_L = i_L/A$) is equal to the catalytic current density (j_{cat}) at $E = 0.300$ V *vs.* $E^{o'}$. As D_{Ac} is decreased, the limiting current density decreases and the voltammograms deviate from the sigmoid shape (*i.e.* can no longer be fit to eqn (37)) In Fig. 3I, each voltammogram is normalized by its own limiting current to emphasize the deviation in shape as D_{Ac} is decreased.

is greater than the rate of Step 3, the significance of which is described in Cases 2 and 3 below). Fig. 3A and 3B demonstrate that, for Case 1, it is numerically possible for acetate to become depleted within the biofilm before it reaches layers closest to the electrode surface. A finite mass transport rate of acetate into the biofilm from the medium may therefore result in an upper limit to the biofilm thickness, defined by the diffusion depth of acetate into the biofilm from the medium (Fig. 3A and 3B) and characterized by: decreasing metabolic activity, $(S_{Ac})_z$, as $z \rightarrow 0$ (Fig. 3C and 3D); a decreasing rate of proton generation, $(S_{H^+})_z$, as $z \rightarrow 0$ (Fig. 3E and 3F); and a proton concentration gradient in which pH within the biofilm is expected to decrease as $z \rightarrow L$. When the depletion of acetate is not appreciable (*e.g.* $D_{Ac} > 4$ in Fig. 3A–3I) such that metabolic activity across the biofilm with respect to proton generation is constant, solution of eqn (16)–(19) yields:

$$[H^+]_z = [H^+]^* - \frac{S_{H^+}}{D_{H^+}} z^2 \quad (35)$$

where

$$\frac{d[H^+]_0}{dz} = 0 \quad (36)$$

And where S_{H^+} is the rate of proton generation by each layer when uniform across the biofilm, $\frac{d[H^+]_z}{dz} \rightarrow 0$ as $z \rightarrow 0$ owing to lack of proton generation by the electrode, and $[H^+]_z \rightarrow [H^+]^*$ as $z \rightarrow L$ (Fig. 3G, $D_{Ac} = 9$). When the depletion of acetate is appreciable such that $(S_{H^+})_z$ decreases as $z \rightarrow 0$ (*e.g.* $D_{Ac} < 4$ in Fig. 3A–3I), an explicit solution for eqn (16)–(19) is not obtainable. When numerically solved, the resulting proton gradient is mitigated but present as long as protons are generated in the biofilm (Fig. 3G, $D_{Ac} = 3$). If the buffer participates in proton mass transport out of the biofilm, we can infer that it will preferentially reduce $[H^+]_z$ as $z \rightarrow L$ depending upon the diffusion depth of buffer into the biofilm from the medium, still resulting in a proton gradient for finite values of $[B]^*$, and K_{eq}. Fig. 3H and 3I depict the corresponding dependency of current on D_{Ac} by voltammetry for $v \rightarrow 0$ (approximated by $v = 0$) based on numerical solution of eqn (3). For relatively large values of D_{Ac} when $K_M \ll 8[Ac]_z$ throughout the biofilm (Fig. 3A), this voltammetry exhibits a sigmoid-shaped i_{cat} *vs.* E dependency defined as:

$$i_{cat} = \frac{i_L X'}{1 + X'} \quad (37)$$

where

$$X' = e^{\left[\frac{(E-E_M)}{f}\right]} \quad (38)$$

and where i_L is the maximum value of i_{cat} (when $E \gg E_M$), and E_M is the midpoint potential where $i_{cat} = \frac{i_L}{2}$. Solving eqn (34) for E_M yields (when $v = 0$):

$$E_M = E^{0'} + \frac{RT}{nF} \ln\left(\frac{k_{cat}}{k\Gamma_{Med} + k_{cat}}\right) \quad (39)$$

As D_{Ac} is decreased, this voltammetry exhibits a characteristic deviation from the idealized sigmoid-shape and a decreasing limiting current (i_L).

Case 2: catalytic current limited by Step 2. When the rates of Steps 1, 3, 4 and 5 are infinitely fast and there is excess acetate such that $K_M \ll 8[Ac]_z$ throughout the biofilm, if the rate of Step 2 limits catalytic current, then

$$\frac{k_{cat}\Gamma_{\mathrm{Mic}}}{k\Gamma_{\mathrm{Med_{ox}}}\Gamma_{\mathrm{Mic}}} = \frac{k_{cat}}{k\frac{\Gamma_{\mathrm{Med}}\mathrm{X}}{1+\mathrm{x}}} \ll 1 \quad (40)$$

where k_{cat} is the rate of Step 2 and $k\frac{\Gamma_{\mathrm{Med}}\mathrm{X}}{1+\mathrm{x}}\Gamma_{\mathrm{Mic}}$ is the rate of step 3. Since $\Gamma_{\mathrm{Med_{ox}}}$ is dependent on E and scales between 0 and Γ_{Med}, eqn (40) only applies when E is sufficiently positive such that $\Gamma_{\mathrm{Med_{ox}}}$ is sufficiently large to satisfy the inequality. Solving for E that satisfies eqn (40) yields:

$$E \gg E^{o'} + \frac{1}{f} \ln\left(\frac{k_{cat}}{k\Gamma_{Med} + k_{cat}}\right) \quad (41)$$

Substitution of eqn (40) into eqn (8) when assuming there is excess acetate such that $K_M \ll 8[Ac]$ throughout biofilm yields eqn (42) where the rate of generation of reduced mediator by the biofilm is given by the rate of Step 2 when all of the mediator in the biofilm is in the oxidized form due to the relatively positive electrode potential.

$$S_{\mathrm{Med_{red}}} = k_{cat}\Gamma_{\mathrm{Mic}} \quad (42)$$

Solution of eqn (3) then yields:

$$i = i_{cat} + i_{dE} = nfAk_{cat}\Gamma_{\mathrm{Mic}} + \frac{nfFAv\Gamma_{Med}(X)}{(1+X)^2} \quad (43)$$

when $E - E^{o'}$ is sufficiently large to satisfy eqn (40) where the catalytic current component is proportional to the rate of Step 2 (eqn (34)) for all values of E. Fig. 4 depicts a representative calculated voltammetric scan rate dependency for Case 2 based on eqn (38). Case 2 results in sigmoid-shaped voltammograms as $v \rightarrow 0$ where the limiting current is given by:

$$i_L = nfAk_{cat}\Gamma_{\mathrm{Mic}} \quad (44)$$

when $E - E^{o'}$ is sufficiently large to satisfy eqn (40). Here i_L is proportional to the rate of Step 2 when all the mediator in the biofilm is in the oxidized form due to the relatively positive electrode potential, and the midpoint potential E_M, given by eqn (37), shifts negative of $E^{o'}$ as the rate of Step 2 is made slower relative to Step 3. As v is increased, i_{dE} becomes non-negligible, resulting in a current that is the series addition of i_{cat} and i_{dE}. Notable features of voltammetry for Case 2 are: $E_M \ll E^{o'}$; i_L that scales linearly with k_{cat} and Γ_{mic}; $j_{P,A}$ and $j_{P,C}$ that scale linearly with v and Γ_{Med} for $v \gg 0$ and that converge to $j_{P,A}$ and $j_{P,C} = j_L$ as $v \rightarrow 0$; and $E_{P,A}$ and $E_{P,C} \ll E^{o'}$ for all v. Since there is no acetate or oxidized mediator concentration gradients within the biofilm for Case 2, there is no expected limit to the biofilm thickness. If a finite diffusion value for D_{H^+} is assumed, the resulting proton concentration gradient is described by eqn (35)

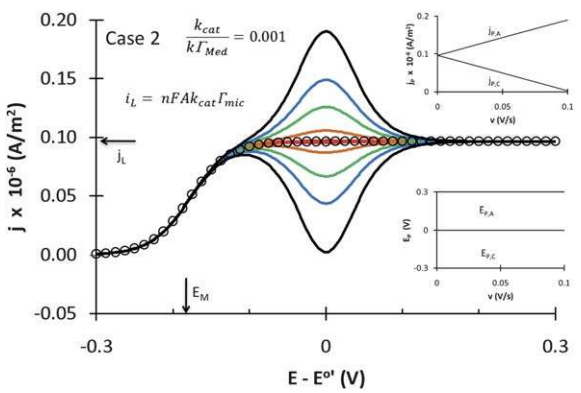

Fig. 4 Representative calculated cyclic voltammograms as a function of scan rate based on Case 2. Scan rate legend same as Fig. 2 where the limiting current is proportional to the rate of Step 2. Insets depict peak current density and peak potential dependency on scan rate values of other parameters used: $A = 1$ cm^2, $\Gamma_{Mic} = 1$ mole cm^{-2}, $\Gamma_{Med} = 1$ mole cm^{-2}, $[Ac]^* = 10\,000$ mole cm^{-3}, $K_M = 1$ mole cm^{-3}, $k_{cat} = 1000$ s^{-1}, $k = 1$ mole^{-1} cm^2 s^{-1}, $k^0 = 10\,000$ s^{-1}, $T = 298$ K. (○): Fit to voltammogram when $v = 0.001$ V s^{-1} based on eqn (37) where E_M is shifted negative of $E^{o'}$.

as depicted in Fig. 3G, $D_{H^+} = 9$, owing to the uniform rate of proton generation in the biofilm. Fig. 5 depicts a representative calculated dependency of E_M on $\frac{k_{cat}}{k\Gamma_{Med}}$ when there is excess acetate as exhibited by slow scan voltammetry based on eqn (34) when $i_{dE} = 0$.

Case 3: catalytic current limited by Step 3. Alternatively, if the rate of Step 3 limits catalytic current when the rates of Steps 1, 2, 4 and 5 are infinitely fast and there is excess acetate such that $K_M \ll 8[Ac]_z$ throughout the biofilm, then

$$\frac{k_{cat}\Gamma_{\mathrm{Mic}}}{k_{\mathrm{Med_{ox}}}\Gamma_{\mathrm{Mic}}} = \frac{k_{cat}\Gamma_{\mathrm{Mic}}}{k\dfrac{\Gamma_{\mathrm{Med}}\mathrm{X}}{1+\mathrm{x}}\Gamma_{\mathrm{Mic}}} \gg 1 \qquad (45)$$

Solving for eqn (3) yields:

$$i = i_{cat} + i_{dE} = \frac{nFA\Gamma_{Mic}k\Gamma_{Med}X}{1+X} + \frac{nfFAv\Gamma_{Med}(X)}{(1+X)^2} \qquad (46)$$

for all values of E where catalytic current is proportional to the rate of Step 3 where the concentration of oxidized mediator throughout the biofilm depends directly on the electrode potential (eqn (30)). Fig. 6 depicts a representative calculated voltammetric scan rate dependency for Case 3 based on eqn (45). Case 3 results in sigmoid-shaped voltammograms as $v \to 0$ where the limiting current, i_L,

$$i_L = nFA\Gamma_{Mic}k\Gamma_{Med} \qquad (47)$$

is proportional to the rate of Step 3 when all of the mediator in the biofilm is in the oxidized form due to the relatively positive electrode potential. As v is increased, i_{dE} becomes non-negligible, resulting in i that is the series addition of i_{cat} and i_{dE}. Notable features of voltammetry under Case 3 are: $E_M = E^{o'}$; i_L that scales linearly with Γ_{Mic}, k, and Γ_{Med}; $j_{P,A}$ and $j_{P,C}$ that scale linearly with v and Γ_{Med} for $v \gg 0$ and converge to $j_{P,A} = j_L$ and $j_{P,C} = 0$ as $v \to 0$; and $E_{P,A}$ and $E_{P,C}$ that converge to $E^{o'}$ for $v \gg 0$. As in Case 2, since there are no Ac or concentration gradients within the biofilm for Case 3, there is no expected limit to the biofilm thickness. Since $(S_{H^+})_z$ is constant throughout the biofilm, a proton concentration gradient will take the form of those depicted in Fig. 3G, $D_{H^+} = 9$.

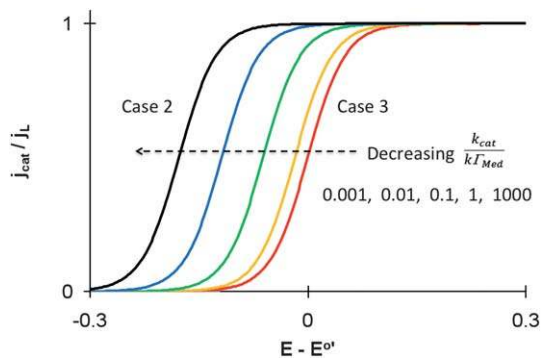

Fig. 5 Representative calculated cyclic voltammograms as a function $\frac{k_{cat}}{k\Gamma_{Med}}$ at slow scan rate ($v = 0.001\,V/s$) based on Case 2. As $\frac{k_{cat}}{k\Gamma_{Med}}$ is decreased, E_M shifts negative of $E^{o'}$. k_{cat} was made progressively smaller while $k\Gamma_{Med}$ was held constant. For each voltammogram, current density is normalized by its limiting current density.

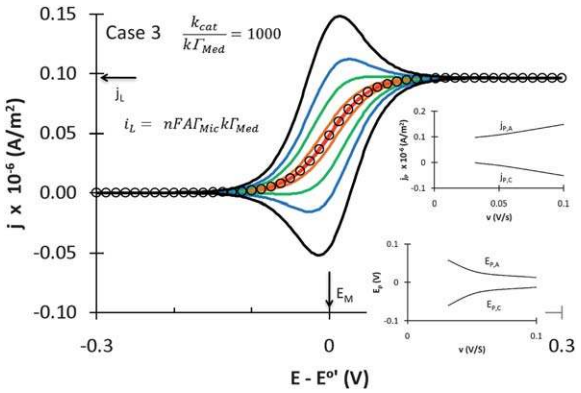

Fig. 6 Representative calculated cyclic voltammograms as a function of scan rate based on Case 3. Scan rate legend same as Fig. 2. Insets depict peak current density and peak potential dependency on scan rate. Values of other parameters used: $A = 1$ cm^2, $\Gamma_{Mic} = 1$ mole cm^{-2}, $\Gamma_{Med} = 1$ mole cm^{-2}, $[Ac]^* = 10\,000$ mole cm^{-3}, $K_M = 1$ mole cm^{-3}, $k_{cat} = 1000$ s^{-1}, $k = 1$ mole^{-1} cm^2 s^{-1}, $k^0 = 10\,000$ s^{-1}, $T = 298$ K. (○): Voltammogram when $v = 0.001\,V/s$ fit to eqn (37) where $E_M = E^{o'}$. No concentration gradients are depicted since none are expected for Case 3. Case 3 does not therefore predict a finite biofilm thickness.

Case 4: catalytic current limited by extracellular electron transport. A finite rate of ET through the biofilm will result in a transient concentration gradient of oxidized mediator across the biofilm during voltammetry in which $(\Gamma_{Med_{ox}})_z$ decreases as $z \to L$ (due to generation of oxidized mediator by the electrode and its reduction by microbes closer to the electrode surface). As a result, is not possible to derive an expression for the full i *vs.* (E,v) voltammetric scan rate dependency as above. Instead, a i *vs.* E dependency for $v \to 0$ (slow scan voltammetry) can be approximated numerically by determining current for each value of E when $v = 0$ (steady state approximation where all concentration gradients in the biofilm are assumed to be constant with time and $i_{dE} = 0$) by setting $\frac{d(\Gamma_{\mathrm{Med_{red}}})_z}{dt} = 0$ and $\frac{d([\mathrm{Ac}])_z}{dt} = 0$. Fig. 7A and 7B depict representative calculated oxidized mediator concentration gradients as a function of D_{et} and E for Case 4 when the rates of Steps 1, 2, 3, and 5 are assumed to be infinitely fast and there is excess acetate such that $K_M \ll 8[Ac]$ throughout the biofilm. Fig. 7A and 8B demonstrate that, for Case 4, it is numerically possible for Med_{ox} to become depleted within the biofilm before it reaches layers closest to the biofilm/medium interface. A finite rate of mass transport of Med_{ox} into the biofilm from the electrode may therefore result in an upper limit to the biofilm thickness, defined by the penetration depth of Med_{ox} into the biofilm from the electrode surface (Fig. 7A and 7B) and characterized by: decreasing metabolic activity, $(S_{Med_{ox}})_z$, as $z \to L$ (Fig. 7C and 7D); a decreasing rate of proton generation, $(S_{H^+})_z$, as $z \to L$ (Fig. 7E and 7F); and a proton concentration gradient in which pH within the biofilm is expected to decrease as $z \to 0$ (Fig. 7G). Fig. 7H and 7I depict the corresponding dependency of current on D_{et} by voltammetry for $v \to 0$ (approximated by $v = 0$) based on the numerical solution of eqn (3). Notable features of this voltammetry are the lack of deviation from the idealized sigmoid-shape of the i_{cat} *vs.* E dependency and i_L that decreases with decreasing D_{et}.

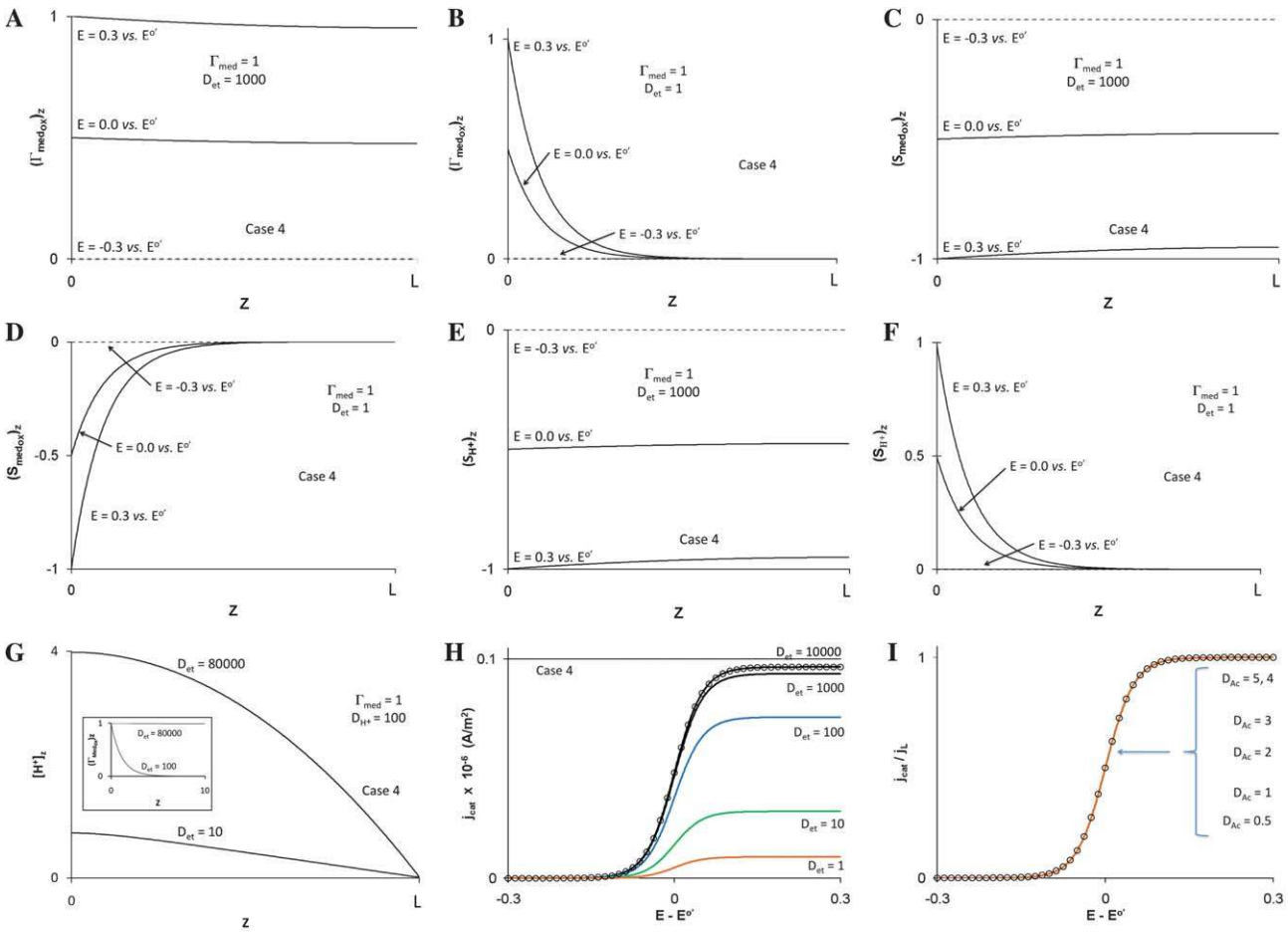

Fig. 7 **(A and B).** Representative calculated steady-state oxidized mediator concentration gradients as a function of the electrode potential and the electron-transfer mediator diffusion coefficient (D_{et}, units of cm^2 s^{-1}) based on Case 4. Horizontal axis is distance inside biofilm from the electrode surface (units of cm). When values of other parameters are maintained constant, a smaller value of D_{et} and a more positive value of E predicts a steeper $\Gamma_{Med_{ox}}$concentration gradient away from the electrode surface. Values of other parameters used: $A = 1$ cm^2, $\Gamma_{Mic} = 1$ mole cm^{-2}, $\Gamma_{Med} = 1$ mole cm^{-2}, $[Ac]^* = 10\,000$ mole cm^{-3}, $K_M = 1$ mole cm^{-3}, $k_{cat} = 1000$ s^{-1}, $k = 1$mole^{-1} cm^2 s^{-1}, $k^0 = 10\,000$ s^{-1}, $T = 298$ K. **(C and D).** Corresponding representative calculated steady-state rate of oxidized mediator consumption gradients based on Case 4. Horizontal axis is distance inside biofilm from the electrode surface (units of cm). Unlike acetate, the rate of consumption of oxidized mediator is assumed 1st order and therefore the rate of oxidized mediator consumption scales linearly with the concentration of oxidized mediator in biofilm. Since oxidized mediator is generated by the electrode, the rate of oxidized mediator consumption drops with increasing distance to the electrode surface. Case 4 therefore predicts a finite biofilm thickness limited by the diffusion depth of oxidized mediator from the electrode into the biofilm. **(E and F).** Corresponding representative calculated steady-state rate of proton generation gradients based on Case 4. Horizontal axis is distance inside biofilm from the electrode surface (units of cm). **(G).** Representative calculated steady-state proton concentration gradients based on Case 4 at $E = 0.3$ V when depletion of oxidized mediator is appreciable ($D_{et} = 10$ cm^2 s^{-1}) and not appreciable ($D_{et} = 10$ cm^2 s^{-1}). Vertical axis is proton concentration in biofilm *vs.* proton concentration in medium. Horizontal axis is distance inside biofilm from the electrode surface (units of cm). **Inset**: corresponding oxidized mediator concentration gradients. Values of other parameters used are same as in Fig. 7A–7F. **(H and I).** Corresponding representative calculated steady-state slow scan cyclic voltammograms (for $v \rightarrow 0$) as a function of the electron-transfer mediator diffusion coefficient (D_{et}, units of cm^2 s^{-1}) based on Case 4. Values of other parameters used: $A = 1$ cm^2, $\Gamma_{Mic} = 1$ mole cm^{-2}, $\Gamma_{Med} = 1$ mole cm^{-2}, $[Ac]^* = 10\,000$ mole cm^{-3}, $K_M = 1$ mole cm^{-3}, $k_{cat} = 1000$ s^{-1}, $k = 1$ mole^{-1} cm^2 s^{-1}, $k^0 = 10\,000$ s^{-1}, $T = 298$ K. (○): Voltammogram when $D_{et} = 10\,000$ cm^2 s^{-1} fit to eqn (37) where $E_M = E^{0'}$. As D_{Ac} is decreased, the limiting current density ($j_L = i_L/A$) decreases but the voltammogram retains its sigmoid shape. In Fig. 7J, each voltammogram is normalized by its own limiting current to emphasize the retention of the sigmoid shape.

Case 5: catalytic current limited by Step 5

If the rate of Step 5 limits catalytic current when the rates of Steps 1–4 are infinitely fast and there is excess acetate such that $K_M \ll 8[Ac]_z$ throughout the biofilm, $k_{ox}$and k_{red} cannot be considered infinite. As a result, it is not possible to derive an expression for the full *i vs.* (E,v) voltammetric scan rate dependency as above since the Nernst equation can not be used to determine $(\Gamma_{\mathrm{Med_{ox}}})_0$ based on E as in Cases 1–4. Instead, for $v \rightarrow 0$ (approximated here by $v = 0$), the rate of generation of Med_{ox} by Step 5 will equal the rate of consumption of Med_{ox} by Step 3 as described by eqn (48) (steady state approximation):

$$k_{ox}\Gamma_{Med_{ox}} - k_{red}\Gamma_{Med_{red}} = \frac{k_{cat}\Gamma_{Mic}}{1 + \dfrac{k_{cat}}{k\Gamma_{Med_{red}}}} \qquad (48)$$

which yields a unique solution for $\Gamma_{Med_{ox}}$ and $\Gamma_{Med_{red}}$ and thus i_{cat} as a function of E for fixed values of k^0, $\propto$, k_{cat}, Γ_{Mic}, k, and Γ_{Med}. Because k_{ox} and k_{red} scale with k^0 (eqn (4) and 5), a finite

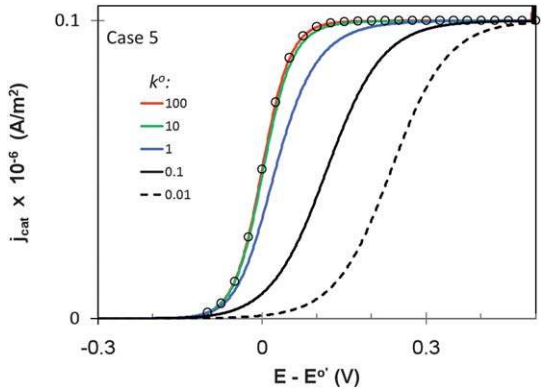

Fig. 8 Representative calculated steady-state slow scan voltammograms (as $v \rightarrow 0$) as a function of the standard heterogeneous electron-transfer rate constant (k^0, units of s^{-1}) based on Case 5. Values of other parameters used: $A = 1$ cm², $\Gamma_{Mic} = 1$ mole cm^{-2}, $\Gamma_{Med} = 1$ mole cm^{-2}, $[Ac]^* = 10\,000$ mole cm^{-3}, $K_M = 1$ mole cm^{-3}, $k_{cat} = 1000$ s^{-1}, $k = 1$ mole^{-1} cm² s^{-1}, $k^0 = 10\,000$ s^{-1}, $T = 298$ K. (○): Fit to voltammogram when $k^0 = 100$ based on eqn (35) where $E_M = E^{o'}$. As k^0 is decreased, the limiting current density remains the same but the voltammograms deviate from the sigmoid shape.

value for k^0 results in a finite biofilm thickness owing to the linear dependency of Γ_{Mic} on thickness. Fig. 8 depicts representative calculated voltammetry for $v \rightarrow 0$ (approximated by $v = 0$) for Case 5. Notable features of this voltammetry is a characteristic deviation from the idealized sigmoid-shape i_{cat} *vs.* E dependency and i_L that is independent of k^0. As in Case 2 and 3, there are no Ac or concentration gradients within the biofilm for Case 5. Since $(S_{H^+})_z$ is constant throughout the biofilm, a proton concentration gradient will take the form of that depicted in Fig. 3G for $D_{Ac} = 9$. It is important to note here that cyclic voltammetry reported for an anode grown biofilm of a DL1 OmcZ (outer surface c-type cytochrome z) deletion mutant[22] and for *Shewanella oneidensis* MR-1[29] exhibit linear features that are consistent with Case 5.

Comparison of simulated voltammetry to experimental voltammetry

Qualitative fit of experimental voltammetry. Fig. 9A and 10A depict experimental cyclic voltammetry recorded at 0.001 V s^{-1} of anodes modified with fully grown biofilms of strains DL1 and KN400. Values for E_M and j_L were determined for each by qualitatively fitting the cathodic voltammetric scan to eqn (37) (the deviation in current depicted in the anodic voltammograms is discussed below). Fitting was performed by first matching j_L then determining E_M from the value of E where $j_{cat} = \frac{j_L}{2}$.

DL1 anode-modified biofilms exhibited a mean E_M of −0.365 ± 0.005 V *vs.* Ag/AgCl that ranged from −0.350 to −0.380 V with a standard deviation of 0.013 V; and a mean j_L of 3.97 ± 0.02 A m^{-2} that ranged from 3.45 to 4.65 A m^{-2} with a standard deviation of 0.72 A m^{-2} (18.2% of the mean). This value is consistent with E_M of −0.150 V (*vs.* SHE) previously reported for *G. sulfurreducens* strain DL1.[22] KN400 anode-modified biofilms exhibited a mean E_M of −0.370 ± 0.005 V *vs.* Ag/AgCl that ranged from −0.345 to −0.380 V with a standard deviation of 0.016 V; and a mean $j_L$of 7.48 ± 0.02 A m^{-2} that ranged from 4.65 to 8.70 A m^{-2} with a standard deviation of 0.862 A m^{-2}

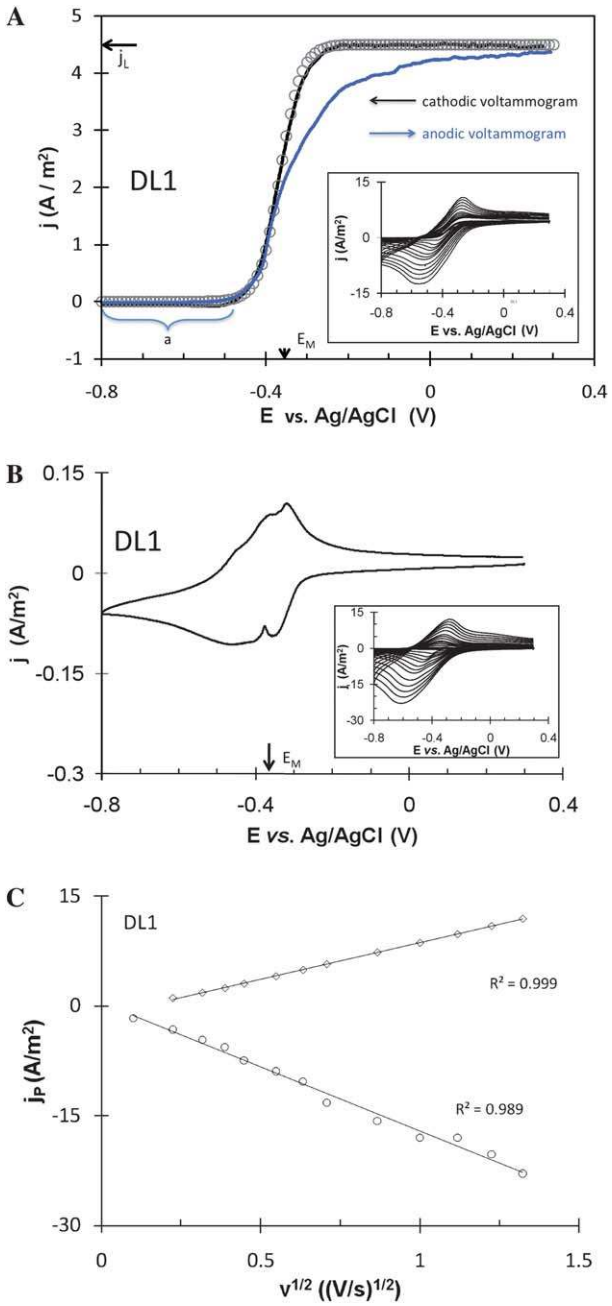

Fig. 9 **(A).** Representative slow scan experimental cyclic voltammogram of a DL1 biofilm-modified anode; $v = 0.001$ V s^{-1}, $A = 0.03$ cm², $T = 303$ K. (○): Cathodic scan fit to eqn (37). Insets depicts scan rate dependency for $v = 0.001$ to 2.00 V s^{-1}. **(B).** Same as Fig. 9A recorded following acetate depletion. **(C).** Scan rate dependency of peak currents of voltammograms depicted in Fig. 9B.

(11.5% of the mean). For all intents and purposes, E_M of DL1 and KN400 are considered identical, while j_L is, on average, 1.9-fold higher for KN400 than DL1, even though the total biomass of the biofilms was approximately the same (data not shown). Impedance spectroscopy (data not shown) indicated that the midpoint potentials of the biofilm-modified anodes depicted in Fig. 9A and 10A are within ±0.01 V of $E^{o'}$ of their ET mediators associated with the terminal ET reaction (Step 5) based on minimization of charge transfer resistance.[51]

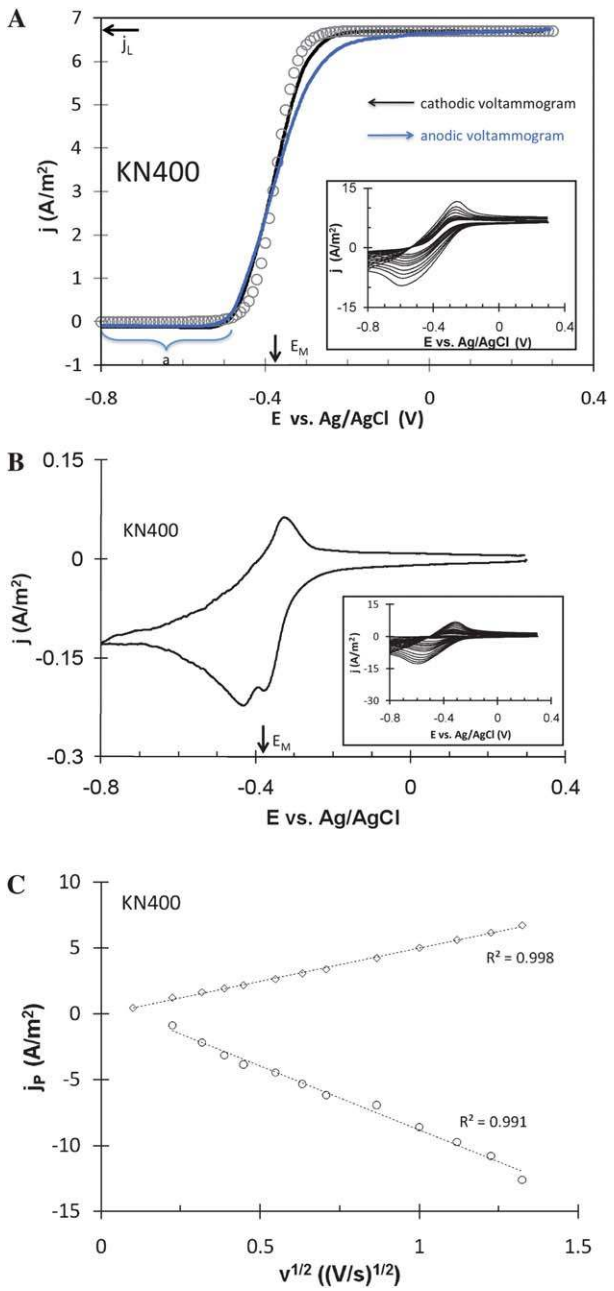

Fig. 10 **(A).** Same as Fig. 9A, but for a KN400 biofilm-modified anode. **(B).** Same as Fig. 10A recorded following acetate depletion. **(C).** Scan rate dependency of peak currents of voltammograms depicted in Fig. 10B.

Voltammetry recorded at 0.002 V s^{-1} in the absence of acetate (non-turnover) exhibits anodic and cathodic peaks with peak potentials in close proximity to the E_M for each of the biofilm-modified anodes (Fig. 9B and 10B). The presence of more than one peak may result from a population of a single redox active molecule that accepts multiple electrons; multiple redox active molecules, including ET mediator(s), that exhibit different formal potentials; or from the same redox active molecule occupying different micro-environments at the biofilm/electrode interface.[52] Based on their shape, the set of peaks at the more positive potential appears to be associated with redox molecules whose current is not affected by diffusion (*e.g.* Fig. 2), while the set of peaks at the more negative potential appears to be associated with redox molecules whose current is affected by diffusion.[47] Such a scenario can arise, for example, if a portion of a population of identical redox molecules near the electrode surface ($z = 0$) becomes physically adsorbed to the electrode surface when reduced, and desorbs when oxidized. This phenomenon will result in an adsorption (diffusion-less) voltammetric pre-peak at a more positive potential, owing to the lower free energy of the reduced form of the redox species when adsorbed.[53] Such pre-waves are often characterized by a sharp cleft between cathodic peaks due to depletion of the redox molecules by adsorption that decreases the concentration of subsequently reduced non-adsorbed molecules. It is also possible to generate voltammograms similar in form to Fig. 9B and 10B from a population of identical redox molecules confined to a thin film bound to an electrode surface when the concentration of redox molecules is relatively high, resulting in lateral electron-transfer among adjacent mediators parallel to the electrode surface.[54]

The ability to qualitatively fit the cathodic voltammograms of both biofilm-modified anodes to eqn (37) suggests that catalytic current is not limited by mass transport of acetate through the biofilm as described by Case 1 or the rate of ET across the biofilm/electrode interface as described by Case 5. If either were rate-limiting, we would expect to see the characteristic deviations in slow scan voltammograms depicted in Fig. 3H, 3I and 8. Availability of acetate throughout the entire biofilm is consistent with reports that transcript abundance of genes upregulated during acetate limitation were not significantly different at various depths throughout anode-respiring biofilms of *G. sulfurreducens*.[55] In addition, the apparent convergence of E_M with $E^{o'}$ as described above suggests that the rate of Step 2 is much faster than the rate of Step 3. Therefore, Step 2, the microbial turnover of acetate to protons and CO_2, is not contributing to current limitations.

Current is limited by either intracellular ET to the mediator pool (Step 3) or ET between bound mediators in the extracellular environment (Step 4). The ability to qualitatively fit Fig. 9 and 10 to eqn (37) suggests that catalytic current generated by biofilm-modified anodes of either *G. sulfurreducens* strain DL1 or strain KN400 is limited by Step 3 or Step 4. Both DL1 and KN400 form biofilms on anodes that achieve a self-determined maximum thickness.[20] Case 3 does not provide a theoretical upper limit to biofilm thickness because neither acetate nor oxidized mediator would be depleted within the biofilm.

In contrast to Case 3, Case 4 provides a theoretical basis for the finite thickness obtained by these biofilms because it implies that the available pool of oxidized extracellular ET mediator decreases when $z \rightarrow L$. The resulting accumulation of reduced mediator in the outer portions of the biofilm predicted by the model for Case 4 is consistent with the proposed capacitance of *G. sulfurreducens* afforded by its abundant cytochromes.[56] As the mediator pool of the biofilm becomes more reduced, a lack of available oxidized ET mediator to accept electrons will limit growth as cells attempt to conserve energy by storing electrons and slowing down biomass production.[57] This prediction is also consistent with transcriptional analysis of anode-respiring

biofilms of strain DL1 performed at various distances from the electrode surface, revealing a slight, but non-negligible decrease in expression of genes for ribosomal proteins and genes for proteins involved in extracytoplasmic electron transfer.[55] The point at which the availability of oxidized extracellular ET mediator (*e.g.* electron acceptor) becomes limiting could therefore be the theoretical upper-limit of biofilm thickness.

While anode-grown biofilms of KN400 were found to have an average total protein content comparable to identically grown DL1 biofilms, strain KN400 has been reported to contain significantly less outer surface *c*-type cytochromes than strain DL1, and develop to roughly half the average biofilm thickness.[16] This is surprising given that transcriptional and mutant analysis of anode-respiring biofilms of *G. sulfurreducens* have identified a number of redox active proteins, in particular OmcZ, important for establishing maximum current density on an electrode.[20] A thinner KN400 biofilm with a similar protein content to that of the thicker DL1 biofilm suggests that the cells may be more densely packed, bringing ET mediators into closer proximity, and that differences in thickness may be attributed to differences in the extracellular polysaccharide (EPS) matrix between the two biofilms.[16] A lower abundance of *c*-type cytochromes may be compensated for in KN400 by an apparent increase in pili, outer-surface appendages implicated in long-range electron transfer, and recently shown in strain DL1 to localize some outer surface *c*-type cytochromes along their length when grown on Fe(III) oxide.[58] Both of these physiological characteristics may alleviate, but not eliminate, rate-limitations attributed to Step 4 if they result in locating more ET mediators within closer proximity to one another in the KN400 biofilm matrix, effectively increasing the pool of available oxidized mediator above that of strain DL1, despite the apparent decrease in cytochrome *c*-type proteins.

The possibility that Step 4 may limit catalytic current is also consistent with a dependency on the square root of scan rate of the voltammetric peak currents (Fig. 9C and 10C) measured from voltammograms of each biofilm recorded under non-turnover conditions (insets, Fig. 9B and 10B). These currents are indicative of EET through the biofilm in the absence of acetate due to the changing electrode potential (i_{dE}). The square root dependency suggests that EET is limited by diffusing charge carriers (*i.e.* soluble ET mediators) or, in the case of *G. sulfurreducens*, diffusing charge (electrons hopping among fixed ET mediators).[44]

Current may be further limited by proton diffusion out of the biofilm (Step 1). For all 5 cases of our model, a proton concentration gradient is assumed to occur due to the finite diffusion coefficients for protons, buffer, and protonated buffer. An inhibitory effect on catalytic current generation by proton accumulation within the biofilm cannot yet be explicitly described by our model since Step 2 is assumed irreversible. Any inhibitory effect may be implicitly described assuming that there is a finite pH range in which DL1 and KN400 are viable.[6,35,59] Proton accumulation inside anode-grown biofilms occurs under current-producing conditions[59] and has been suggested to inhibit metabolic activity of cells close to the electrode surface owing to excessively low pH.[35,59] In the case of *G. sulfurreducens* strain DL1, cells appear to be metabolically active throughout the entire biofilm based on transcriptional analysis of gene expression.[55] However, an increase in transcript abundance for genes involved stress response was observed closer to the electrode surface.[60] According to Fick's first law of diffusion as described above, the thinner biofilm of strain KN400 may also alleviate any current-limitation due to proton accumulation because it will be predicted to have a greater flux of protons out of the biofilm than the thicker DL1 biofilm.[16]

The effects of pH and buffering capacity of the medium on the maximum catalytic current generated by anode biofilms have been demonstrated in MFCs. However, whether these effects arise in the anode biofilm itself, or are attributed to the internal resistance of proton transport between the anode and cathode, including transport across a permeable membrane, has not been determined.[7] For example, Fan and colleagues[6] applied impedance spectroscopy to quantify the internal resistance of MFCs at different pH and buffering capacities and showed that internal resistance is not affected and is small compared to resistances indicative of the anode catalytic process. However, curvature in power density *vs.* current density plots from the same study exhibit significant internal resistances in their MFC system compared to those of analytical MFCs designed to minimize internal resistances.[16]

In order to eliminate the effects of internal resistance, Torres *et al.*,[35] demonstrated the effect of pH on catalytic current density generated by biofilm modified electrodes using a potentiostat in a three-electrode configuration (working, counter, and reference). In this case, steady-state current density *vs.* anode potential dependencies of anode-grown biofilms enriched in *G. sulfurreducens* that were recorded in phosphate-buffered medium exhibit non-ideal behavior when we attempt to fit them to eqn (37) of our model. This non-ideal behavior may in fact be a manifestation of limited proton mass transport out of the biofilm, similar to Cases 1, 2, and 5 above. To be clear, we did not explore the dependency on pH of the biofilms described here, and these experiments are planned for the future.

Deviation in current exhibited by anodic slow scan voltammograms of KN400 biofilms. While the cathodic voltammograms of Fig. 9 and 10 appear nearly ideal, the anodic voltammograms are distorted. This distortion manifests as an onset of negative deviation in catalytic current. It is dependent on the voltammetric scan rate and is more pronounced at 0.002 V s^{-1} (Fig. 11 and 12) but not observable at 0.05 V s^{-1}. The scan rate dependency indicates that the deviation in current is a transient phenomenon resulting in current inhibition that is dependent on the length of time that i_{cat} is maintained near zero during the anodic and cathodic voltammograms (when $E^{o\prime} \leq -0.4$ V *vs.* Ag/AgCl, 80 s at $v = 0.01$ V s^{-1}, longer for slower scan rates) and on length of time recovery is observed during the cathodic voltammogram (longer for slower scan rates). It is our supposition that this deviation is due to a lag in the rate of oxidation of the electrode reduced mediator pool due to limitations by Step 3 of the model. As the anodic scan returns to an oxidizing potential, cellular status switches rapidly from energy conservation to energy metabolism, and reduced electron carriers are not immediately reoxidized. In other words, there is a lag in step 3 where electrons generated from acetate oxidation are more slowly transferred onto the outer surface of the cell.[56]

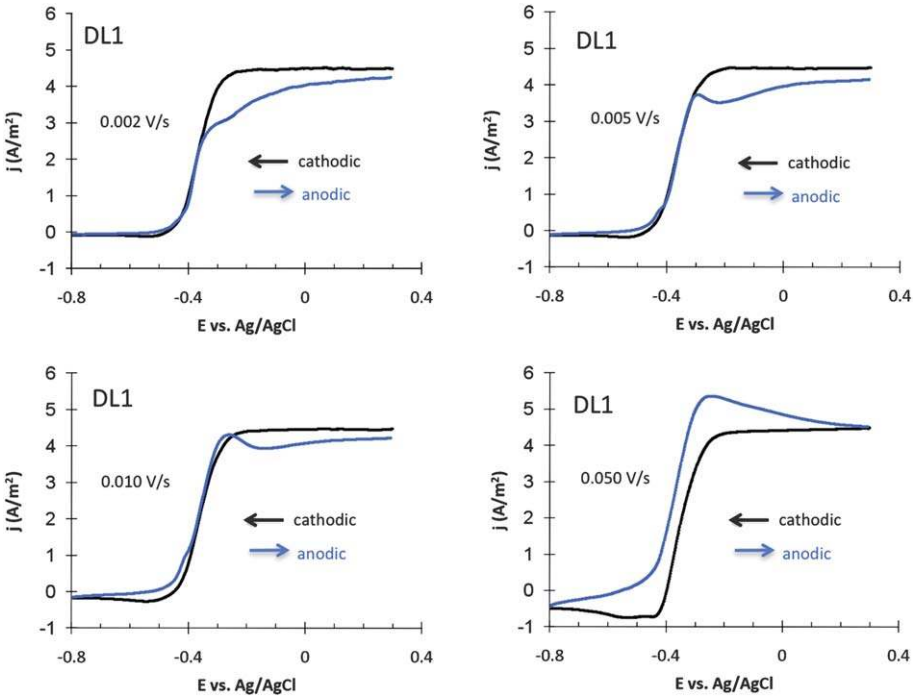

Fig. 11 Same as Fig. 9A, but recorded at indicated scan rates.

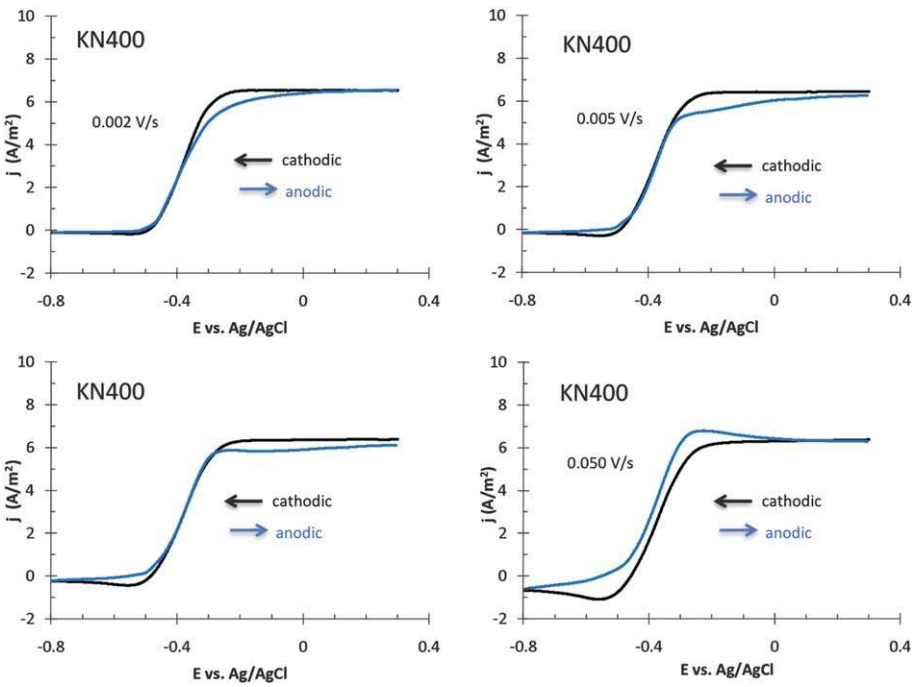

Fig. 12 Same as Fig. 10A, but recorded at indicated scan rates.

Conclusion

Analysis of differential gene expression in anode-respiring biofilms of *G. sulfurreducens* has shown that a number of redox active proteins, as well as pili, are important in establishing maximum current density on an electrode.[20] Results from previous voltammetric analysis of *G. sulfurreducens* wild type and mutant strains lacking these essential components, together with the results we have presented here for strain DL1 and KN400, are consistent with a diffusional model for ET through the biofilm utilizing one or more bound redox species which appear to limit Step 4 of ET, extracellular ET between bound mediators. Although much is known concerning the metabolic state of *G. sulfurreducens* strain DL1 during biofilm growth on an electrode,[19,20,22,55,59] to date very little is known about strain KN400. Therefore, at this time we propose the following

conclusions concerning limiting current for DL1 and KN400 biofilms. 1) Mass transport of reactants into the biofilm (Step 1) does not limit catalytic current in either strain. 2) Mass transport of protons out of the biofilm (Step 1) cannot be ruled out as a limitation to catalytic current in either strain. 3) Microbial turnover of acetate (Step 2) does not limit catalytic current in either strain. 4) Intracellular reduction of electron-transfer mediator (Step 3) does not limit catalytic current in either strain. 5) Step 2 is faster than Step 3 in either strain. 6) Extracellular electron transfer between bound redox mediators (Step 4) limits catalytic current in either strain and this limitation predicts a finite thickness for a biofilm based on finite diffusion depth of electron holes (oxidized mediator) generated at the electrode surface on a biofilm. 7) Electron-transfer across the biofilm/electrode interface (Step 5) does not limit catalytic current in either strain. Voltammetry of the KN400-modified anode depicted in Fig. 9A appears to exhibit a modest deviation from the fit consistent with Case 5. This suggests that Step 5 for KN400 is only moderately fast compared to the scan rate (0.002 V s^{-1}), and surprisingly, is slower than for DL1. This, however, would not limit the maximum catalytic current at the potential we have chosen for analysis (+0.3 V *vs.* Ag/AgCl).

We have developed a model for assessing the current-limiting step in ET through a biofilm of *G. sulfurreducens* when modeled as a classic enzyme-modified electrode. This model has been universally designed for application to biofilms other than *G. sulfurreducens* and should serve as a platform for voltammetric analysis for microbially driven kinetics at both the anode and cathode of microbial fuel cells.

Experimental methods

Culturing conditions

Geobacter sulfurreducens strain DL1 (ATCC#51573) and variant KN400 were obtained from our laboratory culture collection. Both cultures were maintained under anaerobic conditions (N_2 : CO_2, 80 : 20%) with freshwater medium containing fumarate (40 mM) and acetate (10 mM) using previously described methods.[18,61] Freshwater medium contained per liter: 2.5 g sodium bicarbonate ($NaHCO_3$), 0.1 g potassium chloride (KCl), 0.25 g ammonium chloride (NH_4Cl), 0.6 g sodium phosphate dibasic (NaH_2PO_4), 10 ml DL vitamin mixture, and 10 ml DL mineral mixture.[18] Cysteine (10 μM) was added as a reductant.

Electrode systems

All experiments were performed in single-chamber electrochemical cells (250 ml volume) with a 3 mm disk glassy carbon working electrode, graphite rod (0.6 cm diameter, approximately 6 cm length) as the counter electrode, and Ag/AgCl reference electrode. Glassy carbon electrodes were soaked in 0.5 N NaOH for at least 1 h, polished with 6 micron diamond paste (Buehler), sonicated for 30 min, rinsed in deionized water, soaked in 0.5 N HCl for 1 h, and rinsed twice in acetone. Working electrodes and reference electrodes were sterilized by soaking in a 10% bleach solution for 20 min, followed by rinsing in sterile deionized water for 20 min. Counter electrodes were sterilized in partially assembled cells by autoclaving.

Electrochemical cells were inoculated with log-phase *G. sulfurreducens* strain DL1 (3% [v/v] inoculum, O.D. 0.4–0.6) or variant KN400 (2% [v/v] inoculum, O.D. 0.1–0.3) ($n = 5$ for DL1, $n = 4$ for KN400). Single-chamber electrochemical cells were filled (approximately 175 ml) with freshwater medium containing acetate (10 mM) only as the electron donor. The working electrode was held at +300 mV (*vs.* Ag/AgCl) and served as the electron acceptor. Cells were continuously stirred on a setting of "2" (brand of stir plate used) and maintained at 30 °C with a recirculating water bath. Cells were continuously purged with N_2 : CO_2 (80 : 20%) to maintain anaerobic conditions.

Once current was observed to increase (approximately 24 h for variant KN400 and approximately 72 h for strain DL1) cells were placed on flow mode similar to those systems previously described.[4] Briefly, anaerobic freshwater medium containing acetate (10 mM) was continuously supplied to the electrochemical cell using a peristaltic pump (Ismatec) at a dilution rate of 0.1 h^{-1}. All tubing used to supply medium to the electrochemical cell was connected using nickel-plated brass luer-lock connectors (Cole Parmer) and was sterilized by autoclaving. Effluent was collected in a waste container and disposed.

Electrochemical analysis

All potentiostat programs and cyclic voltammetry was performed using a Solartron 1470E multichannel potentiostat (Solartron Analytical) and Multistat software package (Scribner Associates). Under potentiostated conditions the working electrode was held at +0.3 V *vs.* Ag/AgCl. Cyclic voltammetry (CV) was performed prior to inoculation to record background, non-Faradaic current. Parameters for CV were as follows: $E_i = 0.3$ V *vs.* Ag/AgCl; $E_f = -0.8$ V *vs.* Ag/AgCl at the following scan rates in this order: 2000 mV s^{-1}, 1750 mV s^{-1}, 1500 mV s^{-1}, 1250 mV s^{-1}, 1000 mV s^{-1}, 750 mV s^{-1}, 500 mV s^{-1}, 400 mV s^{-1}, 300 mV s^{-1}, 200 mV s^{-1}, 150 mV s^{-1}, 100 mV s^{-1}, 50 mV s^{-1}, 10 mV s^{-1}, 5 mV s^{-1}, 2 mV s^{-1}, 1 mV s^{-1}. Chronoamperometry was performed at E = 0.3 mV *vs.* Ag/AgCl for 1500 s between each scan, which we found to be sufficient to return to the maximum current at +0.3 V (*vs.* Ag/AgCl).

Differential pulse voltammetry (DPV) and electrochemical impedance spectroscopy (EIS) were performed using a model CHI660A potentiostat with CH instruments EC MFC Application software package (CH Instruments, USA). Parameters for DPV were modified from those previously reported [29] and were as follows: $E_{initial}$ (E_i) = −0.755 V *vs.* Ag/AgCl and E_{final} (E_f) = 0.3 V *vs.* Ag/AgCl; pulse height, 50 mV; pulse width 200 ms; step height, 2 mV; step time, 500 ms; scan rate, 2 mV s^{-1}. Electrochemical impedance spectroscopy (EIS) was conducted to confirm the midpoint potential of the terminal electron transfer mediator as described elsewhere in the literature.[29] EIS was performed at ≥ 4 potentials (potentiostatic EIS) determined by changing the potential within 40 mV of the peak potential revealed during DPV (data not shown).

Catalytic current density is normalized by electrode geometric surface area. Use of current density allows direct comparison to experimental data based on electrodes with different surface areas.

Protein analysis

Total protein was determined following completion of all electrochemical measurements. Cell biomass was removed from the surface of the working electrode using a fresh, surface sterilized razor blade. Cells were resuspended in isotonic wash buffer (list components), pelleted at 14 000g for 5 min, resuspended in 5% SDS solution and incubated at 95 °C to solubilize the protein. Total protein was determined using the bicinchoninic acid method (Pierce) with bovine serum albumin (BSA) as a standard.

Computational methods

Simulations were performed using Mathematica and standard numerical methods. In the case of each concentration gradient, the biofilm was divided into thinner and thinner layers until the gradient became independent of layer thickness. In the case of the voltammograms, a 0.0001 V resolution was used.

Abbreviations

A	(a) electrode area (assumed perfectly smooth), units of cm^2. (b) unit of current
α	transfer coefficient
Ac	acetate
$[Ac]$	Ac concentration in biofilm when assumed uniform, units of mole cm^{-3}
$[Ac]$*	Ac concentration in bulk media, units of mole cm^{-3}
$[Ac]_z$	Ac concentration in a thin layer of the biofilm of thickness dz distance z from the electrode surface, units of mole cm^{-3}
$[B]_z$	unprotonated buffer concentration in a thin layer of the biofilm of thickness dz distance z from the electrode surface, units of mole cm^{-3}
$[BH^+]_z$	protonated buffer concentration in a thin layer of the biofilm of thickness dz distance z from the electrode surface, units of mole cm^{-3}
$[B]$*	unprotonated buffer concentration in the medium, units of mole cm^{-3}
$[BH^+]$*	protonated buffer concentration in the medium, units of mole cm^{-3}
D_{Ac}	Ac diffusion coefficient, units of cm^2 s^{-1}
D_{CO_2}	carbon dioxide diffusion coefficient, units of cm^2 s^{-1}
D_{H^+}	proton diffusion coefficient, units of cm^2 s^{-1}
D_B	unprotonated buffer diffusion coefficient, units of cm^2 s^{-1}
D_{BH^+}	protonated buffer diffusion coefficient, units of cm^2 s^{-1}
D_{et}	effective diffusion coefficient of electrons in the biofilm, units of cm^2 s^{-1}
ET	electron transfer
EET	extracellular electron transfer
E	electrode potential, units of V
E_{init}	voltammetric initial E, units of V
$E^{o\prime}$	*Med* formal E, units of V
E_P	peak potential, units of V
E_M	voltammetric midpoint E, units of V
f	$RT/F = 0.02569$ V at $T = 25$ °C
F	Faraday constant
Γ_{Med}	total *Med* concentration in the biofilm, $\int_0^L(\Gamma_{med})_z$, where $\Gamma_{Med}=\Gamma_{Med_{ox}} + \Gamma_{Med_{red}}$, units of units of mole cm^{-2} surface area of the electrode
$\Gamma_{Med_{ox}}$	total Med_{ox} concentration in the biofilm, $\int_0^L(\Gamma_{Med_{ox}})_z$, units of mole cm^{-2} surface area of the electrode
$\Gamma_{Med_{red}}$	total Med_{red} concentration in the biofilm, $\int_0^L(\Gamma_{Med_{red}})_z$, units of mole cm^{-2} surface area of the electrode
$(\Gamma_{Med_{ox}})_z$	Med_{ox} concentration in a thin layer of the biofilm of thickness dz distance z from the electrode surface, units of mole cm^{-2} surface area of the electrode
$(\Gamma_{Med_{red}})_z$	Med_{red} concentration in a thin layer of the biofilm of thickness dz distance z from the electrode surface, units of mole cm^{-2} surface area of the electrode
$(\Gamma_{Mic})_z$	effective concentration of microbes a thin layer of the biofilm of thickness dz distance z from the electrode surface, units of mole cm^{-2} surface area of the electrode
Γ_{Mic}	total effective concentration of microbes in the biofilm, $\int_0^L(\Gamma_{Mic})_z$, units of mole cm^{-2} surface area of the electrode
$[H^+]_z$	proton concentration in a thin layer of the biofilm of thickness dz distance z from the electrode surface, units of mole cm^{-3}
$[H^+]$*	proton concentration in the medium, units of mole cm^{-3}
i	current, units of A
i_{cat}	catalytic current due to Ac oxidation, units of A
i_{dE}	current due to change in $\Gamma_{Med}/\Gamma_{Med}$ due to change in E, units of A
i_L	maximum i_{cat}, units of A
j	i normalized by electrode surface area, units of A cm^{-2}
j_L	i_L normalized by electrode surface area, units of A cm^{-2}
j_P	voltammetric peak i normalized by electrode surface area, units of A cm^{-2}
$j_{P,A}$	voltammetric anodic peak i normalized by electrode surface area, units of A cm^{-2}
$j_{P,C}$	voltammetric cathodic peak i normalized by electrode surface area, units of A cm^{-2}
$(J_{Med_{ox}})_z$	difference in flux of Γ_{Med} into and out of a thin layer of biofilm of thickness dz distance z from the electrode surface, units of mole cm^{-1} s^{-1}
$(J_{Med_{red}})_z$	difference in flux of Γ_{Med} into and out of a thin layer of biofilm of thickness dz distance z from the electrode surface, units of mole cm^{-1} s^{-1}
k	rate constant for microbial reduction of *Med*, units of mole^{-1} cm^2 s^{-1}
k_{cat}	rate constant for microbial turnover of Ac to carbon dioxide and protons, units of s^{-1}

K_{eq}	buffer protonation equilibrium constant, units of mole cm^{-3}
k^0	standard rate constant for electrode–*Med* ET reaction, units of s^{-1}
k_{ox}	rate constant for electrode oxidation of *Med*, units of s^{-1}
k_{red}	rate constant for electrode reduction of *Med*, units of s^{-1}
K_M	microbial affinity for Ac, units of mole cm^{-3}
L	biofilm thickness, units of cm
Med	mediator
Med_{ox}	oxidized *Med*
Med_{red}	reduced *Med*
Mic	microbes in biofilm
Mic_{ox}	oxidized microbes in biofilm
Mic_{red}	reduced microbes in biofilm
n	number of electrons transferred by the electrode–*Med* reaction per equivalent of *Med*
R	gas constant
$(S_{Ac})_z$	rate of Ac consumption in a thin layer of the biofilm of thickness dz distance z from the electrode surface, units of mole cm^{-3} s^{-1}
$(S_{BH^+})_z$	rate of protonated buffer generation in a thin layer of the biofilm of thickness dz distance z from the electrode surface, units of mole cm^{-3} s^{-1}
$(S_{H^+})_z$	rate of proton generation in a thin layer of the biofilm of thickness dz distance z from the electrode surface, units of mole cm^{-3} s^{-1}
S_{H^+}	rate of proton generation by each layer of the biofilm when uniform across the biofilm, units of mole cm^{-3} s^{-1}
$(S_{Med_{ox}})_z$	rate of Med_{ox} consumption in a thin layer of the biofilm of thickness dz distance z from the electrode surface, units of mole cm^{-2} s^{-1}
$(S_{Med_{red}})_z$	rate of Med_{red} generation in a thin layer of the biofilm of thickness dz distance z from the electrode surface, units of mole cm^{-2} s^{-1}
t	time, units of s
T	temperature, units of K
v	voltammetric scan rate, units of V s^{-1}
z	distance of a layer in the biofilm of thickness dz from the electrode surface, $z = 0$ denotes layer closest the electrode surface, $z = L$ denotes layer closest to the medium, $0 \leq z \leq L$ denotes all layers in the biofilm, units of cm
dz	incremental change in z, units of cm

Acknowledgements

This work support by the Naval Research Laboratory (L.M.T.) and the Office of Naval Research (D.R.L.: No. N00014-10-1-0084, L.M.T: Grant No. N00014-10-WX20463).

References

1 D. R. Lovley, *Nat. Rev. Microbiol.*, 2006, **4**, 497–508.
2 D. R. Lovley, *Geobiology*, 2008, **6**, 225–231.
3 B. E. Logan, *Nat. Rev. Microbiol.*, 2009, **7**, 375–381.
4 K. P. Nevin, H. Richter, S. F. Covalla, J. P. Johnson, T. L. Woodard, H. Jia, M. Zhang and D. R. Lovley, *Environ. Microbiol.*, 2008, **10**, 2505–2514.
5 S. Cheng and B. E. Logan, *Proc. Natl. Acad. Sci. U. S. A.*, 2007, **104**, 18871–18873.
6 Y. Fan, H. Hu and H. Lui, *Environ. Sci. Technol.*, 2007, **41**, 8154–8158.
7 Y. Fan, H. Hu and H. Lui, *J Power Res*, 2007, **171**, 348–354.
8 D. R. Bond, D. E. Holmes, L. M. Tender and D. R. Lovley, *Science*, 2002, **295**, 483–485.
9 S. Ishii, K. Watanabe, S. Yabuki, B. E. Logan and Y. Sekiguchi, *Appl. Environ. Microbiol.*, 2008, **74**, 7348–7355.
10 L. M. Tender, C. E. Reimers, H. A. Stecher, D. E. Holmes, D. R. Bond, D. A. Lowy, K. Pilobello, S. J. Fertig and D. R. Lovley, *Nat. Biotechnol.*, 2002, **20**, 821–825.
11 D. E. Holmes, D. R. Bond, R. A. O'Neil, C. E. Reimers, L. R. Tender and D. R. Lovley, *Microb. Ecol.*, 2004, **48**, 178–190.
12 S. Jung and J. M. Regan, *Appl. Microbiol. Biotechnol.*, 2007, **77**, 393–402.
13 H.-S. Lee, P. Parameswaran, A. Kato Marcus, C. I. Torres and B. E. Rittmann, *Water Res.*, 2008, **42**, 1501–1510.
14 Y. Liu, F. Harnisch, K. Fricke, R. Sietmann and U. Schroder, *Biosens. Bioelectron.*, 2008, **24**, 1006–1011.
15 C. I. Torres, R. Krajmalnik-Brown, P. Parameswaran, A. Kato Marcus, G. Wanger, Y. A. Gorby and B. E. Rittmann, *Environ. Sci. Technol.*, 2009, **43**, 9519–9524.
16 H. Yi, K. P. Nevin, B.-C. Kim, A. E. Franks, A. Klimes, L. M. Tender and D. R. Lovley, *Biosens. Bioelectron.*, 2009, **24**, 3498–3503.
17 C. I. Torres, A. Kato Marcus, H.-S. Lee, P. Parameswaran, R. Krajmalnik-Brown and B. E. Rittmann, *FEMS Microbiol. Rev.*, 2010, **34**, 3–17.
18 D. R. Bond and D. R. Lovley, *Appl. Environ. Microbiol.*, 2003, **69**, 1548–1555.
19 D. E. Holmes, S. K. Chaudhuri, K. P. Nevin, T. Mehta, B. A. Methe, A. Liu, J. E. Ward, T. L. Woodard, J. Webster and D. R. Lovley, *Environ. Microbiol.*, 2006, **8**, 1805–1815.
20 K. P. Nevin, B.-C. Kim, R. H. Glaven, J. P. Johnson, T. L. Woodard, B. A. Methé, R. J. DiDonato Jr, S. F. Covalla, A. E. Franks, A. Liu and D. R. Lovley, *PLoS One*, 2009, **4**, e5628.
21 H. Richter, K. McCarthy, K. P. Nevin, J. P. Johnson, V. M. Rotello and D. R. Lovley, *Langmuir*, 2008, **24**, 4376–4379.
22 H. Richter, K. P. Nevin, H. Jia, D. A. Lowy, D. R. Lovley and L. M. Tender, *Energy Environ. Sci.*, 2009, **2**, 506–516.
23 C. Dumas, R. Basseguy and A. Bergel, *Electrochim. Acta*, 2008, **53**, 3200–3209.
24 C. Dumas, R. Basseguy and A. Bergel, *Electrochim. Acta*, 2008, **53**, 5235–5241.
25 K. Fricke, F. Harnisch and U. Schroder, *Energy Environ. Sci.*, 2008, **1**, 144–147.
26 B. A. Methé, K. E. Nelson, J. A. Eisen, I. T. Paulsen, W. Nelson, J. F. Heidelberg, D. Wu, M. Wu, N. Ward, M. J. Beanan, R. J. Dodson, R. Madupu, L. M. Brinkac, S. C. Daugherty, R. T. DeBoy, A. S. Durkin, M. Gwinn, J. F. Kolonay, S. A. Sullivan, D. H. Haft, J. Selengut, T. M. Davidsen, N. Zafar, O. White, B. Tran, C. Romero, H. A. Forberger, J. Weidman, H. Khouri, T. V. Feldblyum, T. R. Utterback, S. E. Van Aken, D. R. Lovley and C. M. Fraser, *Science*, 2003, **302**, 1967–1969.
27 R. Mahadevan, D. R. Bond, J. E. Butler, A. Esteve-Nunez, M. V. Coppi, B. O. Palsson, C. H. Schilling and D. R. Lovley, *Appl. Environ. Microbiol.*, 2006, **72**, 1558–1568.
28 M. V. Coppi, C. Leang, S. J. Sandler and D. R. Lovley, *Appl. Environ. Microbiol.*, 2001, **67**, 3180–3187.
29 E. Marsili, D. B. Baron, I. D. Shikhare, D. Coursolle, J. A. Gralnick and D. R. Bond, *Proc. Natl. Acad. Sci. U. S. A.*, 2008, **105**, 3968–3973.
30 J. J. Calvente, A. Narvaez, E. Dominguez and R. Andreu, *J. Phys. Chem. B*, 2003, **107**, 6629–6643.
31 B. E. Rittmann and P. L. McCarty, *Biotechnol. Bioeng.*, 1980, **22**, 2343–2357.
32 H. T. Chang and B. E. Rittmann, *Environ. Sci. Technol.*, 1987, **21**, 273–280.
33 H. T. Chang and B. E. Rittmann, *Environ. Sci. Technol.*, 1987, **21**, 280–288.
34 B. E. Rittmann and J. A. Manem, *Biotechnol. Bioeng.*, 1992, **39**, 914–922.

35 C. I. Torres, A. Kato Marcus and B. E. Rittmann, *Biotechnol. Bioeng.*, 2008, **100**, 872–881.
36 C. I. Torres, H. S. Lee and B. E. Rittmann, *Environ. Sci. Technol.*, 2008, **42**, 8773–8777.
37 H.-S. Lee, C. I. Torres and B. E. Rittmann, *Environ. Sci. Technol.*, 2009, **43**, 7571–7577.
38 J. Wei, P. Liang, X. Cao and X. Huang, *Environ. Sci. Technol.*, 2010, **44**, 3187–3191.
39 C. Amatore, J.-M. Saveant and D. Tessier, *J. Electroanal. Chem.*, 1983, **147**, 39–51.
40 I. Katakis and A. Heller, *Anal. Chem.*, 1992, **64**, 1008–1013.
41 P. G. Pickup and R. W. Murray, *J. Am. Chem. Soc.*, 1983, **105**, 4510–4514.
42 A. Kato Marcus, C. I. Torres and B. E. Rittmann, *Biotechnol. Bioeng.*, 2007, **98**, 1171–1182.
43 J. Hodak, R. *etc*henique and E. J. Calvo, *Langmuir*, 1997, **13**, 2708–2716.
44 B. A. Gregg and A. Heller, *J. Phys. Chem.*, 1991, **95**, 5970–5975.
45 P. G. Pickup, W. Kutner, C. R. Leidner and R. W. Murray, *J. Am. Chem. Soc.*, 1984, **106**, 1991–1998.
46 D. N. Blauch and J.-M. Saveant, *J. Am. Chem. Soc.*, 1992, **114**, 3323–3332.
47 A. J. Bard and L. R. Faulkner, John Wiley & Sons, Inc., New York, 2001, 2nd Edition.
48 K. B. Gregory, D. R. Bond and D. R. Lovley, *Environ. Microbiol.*, 2004, **6**, 596–604.
49 L. M. Tender, M. T. Carter and R. W. Murray, *Anal. Chem.*, 1994, **66**, 3173–3181.
50 R. W. Murray and D. J. Gross, *J. Electroanal. Chem.*, 1984, **13**, 132–136.
51 C. Gabrielli, H. Takenouti, O. Haas and A. Tsukada, *J. Electroanal. Chem.*, 1991, **302**, 59–89.
52 X. Chen, R. Ferrigno, J. Yang and G. M. Whitesides, *Langmuir*, 2002, **18**, 7009–7015.
53 R. H. Wopschall and I. Shain, *Anal. Chem.*, 1967, **39**, 1514–1527.
54 G. K. Rowe and S. E. Creager, *Langmuir*, 1991, **7**, 2307–2312.
55 A. E. Franks, K. P. Nevin, R. H. Glaven and D. R. Lovley, *ISME J.*, 2010, **4**, 509–519.
56 A. Esteve-Nunez, J. Sosnik, P. Visconti and D. R. Lovley, *Environ. Microbiol.*, 2008, **10**, 497–505.
57 A. Esteve-Nunez, M. Rothermich, M. Sharma and D. R. Lovley, *Environ. Microbiol.*, 2005, **7**, 641–648.
58 C. Leang, X. L. Qian, T. Mester and D. R. Lovley, *Appl. Environ. Microbiol.*, 2010, **76**, 4080–4084.
59 A. Franks, K. Nevin, H. Jia, M. Izallalen, T. Woodard and D. Lovley, *Energy Environ. Sci.*, 2009, **2**, 113–119.
60 A. E. Franks, *FEMS Microbiol. Lett.*, 2010, **307**, 111–112.
61 F. Caccavo, D. J. Lonergan, D. R. Lovley, M. Davis, J. F. Stolz and M. J. McInerney, *Appl Environ Microb*, 1994, **60**, 3752–3759.